



This is a repository copy of *Variations in esker morphology and internal architecture record time-transgressive deposition during ice margin retreat in Northern Ireland.*

White Rose Research Online URL for this paper:
<https://eprints.whiterose.ac.uk/173230/>

Version: Accepted Version

Article:

Stoker, B., Livingstone, S. orcid.org/0000-0002-7240-5037, Barr, I. et al. (3 more authors) (2021) Variations in esker morphology and internal architecture record time-transgressive deposition during ice margin retreat in Northern Ireland. *Proceedings of the Geologists' Association*, 132 (4). pp. 409-425. ISSN 0016-7878

<https://doi.org/10.1016/j.pgeola.2021.03.002>

© 2021 Crown Copyright. This is an author produced version of a paper subsequently published in *Proceedings of the Geologists' Association*. Uploaded in accordance with the publisher's self-archiving policy. Article available under the terms of the CC-BY-NC-ND licence (<https://creativecommons.org/licenses/by-nc-nd/4.0/>).

Reuse

This article is distributed under the terms of the Creative Commons Attribution-NonCommercial-NoDerivs (CC BY-NC-ND) licence. This licence only allows you to download this work and share it with others as long as you credit the authors, but you can't change the article in any way or use it commercially. More information and the full terms of the licence here: <https://creativecommons.org/licenses/>

Takedown

If you consider content in White Rose Research Online to be in breach of UK law, please notify us by emailing eprints@whiterose.ac.uk including the URL of the record and the reason for the withdrawal request.



eprints@whiterose.ac.uk
<https://eprints.whiterose.ac.uk/>

1 **Variations in esker morphology and internal architecture record time-transgressive**
2 **deposition during ice margin retreat in Northern Ireland**

3 Ben J. Stoker^{a,b,*}, Stephen J. Livingstone^b, Iestyn D. Barr^c, Alastair Ruffell^d, Robert D. Storrar^e,
4 Sam Roberson^f

5 *Corresponding author, email address: stokerb@natur.cuni.cz

6 ^aDepartment of Physical Geography and Geoecology, Charles University, Prague, Czechia

7 ^bDepartment of Geography, University of Sheffield, UK, South Yorkshire, Sheffield, Winter Street,
8 S10 2TN

9 ^cDepartment of Natural Sciences, Manchester Metropolitan University, UK, Manchester, Oxford Road,
10 M15 6BH

11 ^dSchool of Natural and Built Environment, Queens University Belfast, UK, Belfast, Elmwood Avenue,
12 BT7 1NN

13 ^eDepartment of the Natural and Built Environment, Sheffield Hallam University, UK, Sheffield,
14 Howard Street, S1 1WB

15 ^fGeological Survey of Northern Ireland, Dundonald House, Belfast, BT4 3SB, UK

16 Keywords: Eskers, Northern Ireland, morphology, sedimentology, deglaciation, meltwater

17 **Abstract**

18 The architecture and evolution of the subglacial hydrological system plays a key role in modulating
19 ice flow. Eskers provide an opportunity to understand subglacial hydrology at a broader perspective
20 than contemporary studies. Recent research has established a morphogenetic classification for eskers,
21 but these studies have been limited to topographically simple regions of a single ice sheet. We present
22 an updated map of esker distribution in Northern Ireland based on 5 m resolution elevation data. We
23 also present a high-resolution map of the glacial geomorphology of SW Northern Ireland, based on
24 ~0.4 m resolution elevation data. Ground Penetrating Radar data from four sites along the >20 km
25 long Evishanoran Esker system in central Northern Ireland are combined with geomorphological
26 observations to provide insight into depositional processes and controls on esker formation. Esker
27 architecture indicates two styles of deposition, including an initial high energy flow event in a
28 subglacial conduit, and delta foreset deposition close to the ice sheet margin during ice margin retreat.
29 These delta foreset deposits can be used to reconstruct former ice margins. We identify that local
30 topographic complexity and geological structures (e.g. faults) are important controls on esker
31 formation. The broad-scale esker architecture remains the same despite variable esker platform
32 morphology, suggesting hydrological conditions alone cannot explain esker morphology. This study
33 provides further evidence that morphogenetic relationships cannot be based solely on remote sensing
34 data and must be supported by robust field observations, especially where post-glacial processes may
35 distort esker morphology (e.g. peat infilling).

36

37 **1.0 Introduction**

38 The distribution of meltwater at the base of ice sheets influences ice motion by modulating basal sliding
39 and deformation of sediments. The influence of water on ice flow depends on the architecture of the
40 subglacial drainage network and how it evolves to accommodate water inputs (e.g. Budd et al., 1979;
41 Alley et al., 1986; Iken and Bindshadler, 1986). Efficient low-pressure networks of discrete channels
42 rapidly drain water to the margin and tend to reduce ice velocity (Hubbard and Nienow, 1997).
43 Inefficient distributed networks (e.g. linked cavities, canals and a porous till layer) result in increased
44 effective pressure, in turn leading to higher ice velocities (Röthlisberger, 1972; Schoof, 2010). Recent
45 observations from beneath the Antarctic and Greenland ice sheets have implicated dynamic subglacial
46 water systems in driving rapid ice-flow variations (Zwally et al., 2002; Bell et al., 2007; Stearns et al.,
47 2008; Bartholomew et al., 2010; Davison et al., 2019).

48 For investigations of subglacial hydrological processes, the imprint of meltwater drainage, recorded on
49 the beds of former ice sheets, has a clear advantage over data from contemporary ice sheets (e.g.
50 borehole surveys) because it is possible to reconstruct the history of meltwater drainage over centennial
51 to millennial time-scales and spatially over metres to hundreds of kilometres. These temporal and spatial
52 scales not only allow a more complete understanding of the architecture and evolution of the subglacial
53 drainage network but are relevant for informing numerical modelling experiments (cf. Greenwood et
54 al., 2016; Hewitt & Creyts, 2019). Eskers are the depositional imprint of drainage through subglacial
55 (R-channels), englacial or supraglacial channels (Price, 1969; Banerjee and McDonald, 1975;
56 Gustavson and Boothroyd, 1987; Brennand, 2000) and are commonly found across the beds of former
57 ice sheets (e.g. Storrar et al., 2014a; Stroeven et al., 2016; Clark et al., 2018). They typically comprise
58 elongate ridges of glaciofluvially deposited sand and gravel that can extend tens to hundreds of
59 kilometres, are usually arranged roughly parallel to former ice flow direction, and range from single
60 ridges to more complex anabranching forms (e.g. Flint, 1930; Brennand, 1994; Burke et al., 2012;
61 Storrar et al., 2015; Perkins et al., 2016). Esker geometry, distribution and sedimentary architecture
62 have been widely used to reconstruct drainage pathways and infer past ice sheet dimensions and
63 dynamics (e.g. Shreve, 1985; Dyke and Prest, 1987; Aylsworth and Shilts, 1989; Hebrand and Åmark,
64 1989; Clark and Walder, 1994; Brennand, 1994, 2000; Warren and Ashley, 1994; Margold et al., 2013;
65 Storrar et al., 2013, 2014a; Livingstone et al., 2015). However, there is still considerable uncertainty
66 over the genesis of eskers, including the extent to which they form time-transgressively or
67 synchronously (e.g. Brennand, 2000; Makinen, 2003; Cummings et al., 2011); the magnitude and
68 frequency of drainage (Burke et al., 2008, 2010, 2012; Livingstone et al., 2016; Drews et al., 2017);
69 and the vertical position in the ice mass (i.e. supraglacial, englacial or subglacial) in which they are
70 deposited (Price, 1969; Fitzsimmons, 1991; Perkins et al., 2016).

71 Understanding how eskers form is important for reconstructing palaeo-ice sheets and providing
72 information on subglacial hydrological processes. In particular, the varied form and architecture of
73 eskers is thought to be controlled by the hydrological properties of the channelised drainage system

74 (Burke et al., 2015; Storrar et al., 2015). For example, recent morpho-sedimentary studies of eskers in
75 southern Alberta, Canada, and mapping of eskers emerging from the front of Breiðamerkurjökull,
76 southeast Iceland, have related abundant meltwater and sediment supply to complex esker systems, and
77 low sediment supply and either high or low meltwater abundance to single ridges of uniform geometry
78 (Burke et al., 2015; Storrar et al., 2015, 2020). A barrier to understanding the formation of eskers at the
79 ice sheet-scale is the relative dearth of sedimentological investigations of these long esker systems.
80 Recent work (e.g. Burke et al., 2012; Perkins et al., 2013) has begun to address this using geophysical
81 investigations of the sedimentary architecture of eskers formed beneath the Cordilleran Ice Sheet. To
82 further investigate the relationship between ice sheet hydrology and esker properties, this paper
83 combines detailed geomorphological, geophysical and sedimentological data to assess controls on the
84 formation of a ~20 km long esker network in Northern Ireland (UK) whose morphology changes down-
85 flow from a complex multi-ridge system to a large single ridge.

86 **2.0 Background**

87 *2.1 Glacial history of Ireland*

88 The early stages of the onset of the Irish Ice Sheet (~ 35 ka) were characterised by incursion of Scottish
89 ice flowing in from the NE, which subsumed localised ice caps over Irish upland massifs (Colhoun,
90 1971; Clark and Meehan, 2001; Greenwood and Clark, 2009b). As Irish ice coalesced with western
91 Scottish ice, the location of the dominant ice dispersal centres migrated to upland areas in the west of
92 Ireland, exerting a strong control on ice flow patterns (Greenwood and Clark, 2009b). Heterogenous
93 growth patterns led to ice sheet sectors reaching their maxima at different times. For example, the
94 western margin reached its maximum position relatively early compared to the southern portion of the
95 ice sheet (Ó Cofaigh and Evans, 2007; Greenwood and Clark, 2009b; Ó Cofaigh et al., 2019). The
96 configuration of ice domes and the geomorphology of the Irish Ice Sheet required ice expansion onto
97 the continental shelf, with the Last Glacial Maximum (LGM; 23 ka – 18 ka) resulting in almost complete
98 terrestrial ice coverage across Ireland (Knight et al., 2004; Ó Cofaigh and Evans, 2007; Bradwell et al.,
99 2008; Greenwood and Clark, 2009a,b; Clark et al. 2018).

100 Deglaciation in Ireland was characterised by the migration of competing ice divides, which resulted in
101 a complex deglacial history (Knight, 2003, 2019; Greenwood, 2009b). The ice sheet fragmented as it
102 retreated into upland dispersal centres such as the Connemara Mountains in Western Ireland and County
103 Donegal to the north (Wilson *et al.*, 2019), or lowland ice domes situated in the Lough Neagh Basin
104 and Omagh Basin (Fig. 1). Ice sheet retreat is thought to have been interspersed with asynchronous
105 phases of localised ice advance or stagnation, likely related to the migration of ice divides (Knight,
106 1999; Knight, 2006; Clark *et al.*, 2012; Callard et al., 2020; Chiverrell *et al.*, 2020). Within central
107 Northern Ireland, the two dominant LGM ice dispersal centres were situated in the Lough Neagh basin,
108 and in the Sperrin Mountain range to the north (Fig. 1) (Knight, 1999). During this period, SW ice flow
109 dominated from an ice dome in the NE Omagh Basin offshore towards Donegal Bay (Fig. 1), indicated

110 by an area of subglacial ribs across the Omagh Basin (Knight and McCabe, 1997). Subglacial ribs across
111 central Northern Ireland often display modification or drumlinisation likely associated with changes in
112 ice flow patterns and subglacial thermal regime (Knight, 1997; Knight and McCabe, 1997). An ice flow
113 reversal occurred during deglaciation when the dominant ice dome over the Omagh Basin migrated SW
114 to the Lower Lough Erne Basin, leading to NE ice flow forming a prominent esker system overlying
115 the subglacial ribs (Knight, 2004). The regional retreat pattern to the SW is documented by a series of
116 meltwater landforms, including eskers. A glacial lake formed between the retreating ice sheet margin
117 and the Sperrin Mountains to the north, resulting in the formation of a series of deltas (Dardis, 1986).
118 The final stages of deglaciation were characterised by localised mountain ice caps, with the last
119 remnants of the Irish Ice Sheet likely located in the mountains of Donegal in the northwest (Greenwood
120 and Clark, 2009b; Smith and Knight, 2011).

121 Research into the meltwater systems of Ireland has a long history stretching back to the late 19th century,
122 and has concentrated on the origin of the large (up to 50 m high) ridges of the Esker Riada system in
123 the Irish Midlands (Sollas, 1896; Gregory, 1912, 1921; Hinch, 1921; Flint, 1930). Theories on the origin
124 of these eskers revolved around whether they were deposited by a sub- or supraglacial river system, or
125 whether they represented deltaic glaciofluvial deposits (Gregory, 1921). More recently, studies have
126 debated whether the Esker Riada system and associated glaciofluvial sediments were deposited by
127 meltwater in an interlobate position, between two retreating ice masses (Warren and Ashley, 1994;
128 Pellicer et al., 2012), or as part of a multi-phase model involving westerly ice sheet retreat, followed by
129 a period of ice sheet readvance from the north (Delaney, 2001a, b, 2002; Delaney et al., 2018). The
130 eskers of central Northern Ireland have been used to reconstruct the migration of ice domes and time-
131 transgressive variations in the subglacial drainage system (Knight, 1997; 2019), but historically, there
132 has been less research focused on them.

133 *2.2 Regional Context and Landform Distribution*

134 Central Northern Ireland incorporates the Sperrin Mountains to the north and the Omagh Basin; a low
135 elevation region of undulating topography, to the south (Fig. 1). The regional geology is varied, with a
136 series of folded and faulted Palaeozoic sandstones and limestones to the south, and crystalline granites
137 and gabbros to the north, with varying degrees of metamorphism across the Tyrone Igneous Complex
138 (Knight, 1997; Chew *et al.*, 2008; Geological Survey Northern Ireland, 2016). A series of three large,
139 subparallel fault lines trend NE-SW and define geological boundaries, while smaller faults with a
140 variety of orientations are also prevalent (Geological Survey Northern Ireland, 2016).

141 A range of glacial landforms have been documented across the region, including meltwater channels,
142 eskers, drumlins and subglacial ribs (Colhoun, 1970; Knight, 2003; Clark et al., 2018). Major moraines
143 are largely absent across central Northern Ireland, being restricted to the present coastline and the
144 continental shelf onto which the Irish Ice Sheet extended (Clark et al., 2018; Ó Cofaigh et al., 2019).
145 An area of subglacial ribs dominates the lowland areas across Central Northern Ireland, with ridge

146 crestlines oriented perpendicular to SW ice flow during the LGM (Knight and McCabe, 1997; Knight,
147 2002). These subglacial ribs are commonly drumlinised or exhibit modification by meltwater, which
148 may have been stored in the lowland area between ridge crestlines (Knight and McCabe, 1997; Knight,
149 2002, 2006). Alongside subglacial ribs, E-W orientated drumlins dominate the lowlands of the Omagh
150 and Lough Erne basins (Knight, 1997, 2003). A prominent esker system located NE of the Lower Lough
151 Erne Basin forms a series of bifurcating ridges in a meltwater valley dissecting the zone of subglacial
152 ribs (Fig. 2a). This system was deposited under NE ice flow during deglaciation to the SW, contrasting
153 with the SW ice flow responsible for the formation of the subglacial ribs (Knight, 2002). Therefore,
154 these eskers represent a reversal of the hydraulic gradient as the ice dome situated over the Omagh
155 Basin migrated towards the Lower Lough Erne Basin (Knight and McCabe, 1997).

156 The present study focuses on a >20 km long complex esker system in County Tyrone, Central
157 Northern Ireland. The esker complex trends out of three meltwater channels cutting through the
158 Fintona Hills to the south, and terminates near the Sperrin Mountains in the north (Figs. 1, 2 and
159 3). The NE sector was mapped in part by Gregory (1925) and termed the Evishanoran Esker. Early
160 debate sought to identify whether deposition was associated with local ice masses from the east, or
161 a larger ice mass from the southwest (Charlesworth, 1926; Gregory, 1926). Here we refer to the
162 entire esker complex as the Evishanoran Esker, including newly mapped segments that were not
163 documented in Gregory (1925). A series of eskers to the SW in the Fintona Hills were likely
164 deposited during a later stage of deglaciation and form a meltwater routeway with the Evishanoran
165 Esker (Knight, 2019).

166 **3.0 Methods**

167 *3.1 Geomorphological mapping*

168 Comprehensive mapping of esker ridges was undertaken for the whole of Northern Ireland. Landform
169 mapping was performed within ArcGIS 10.4.1, using a 5 m resolution digital elevation model (DEM)
170 produced by the Land and Property Services Northern Ireland under MOU205, provided to Queens
171 University Belfast. We also mapped all glacial landforms across the study area of SW Northern Ireland
172 using a ~0.4 m resolution digital surface model (DSM) to provide geomorphological context of the area
173 surrounding the Evishanoran Esker (Fig. 2).

174 Landform identification was based on morphology, association with other features and local
175 topography. Esker crestlines were digitized as polylines to investigate their broad-scale distribution and
176 morphological characteristics. Fan-shaped enlargements located at esker termini were classified as
177 esker fans and digitized as polygons at the break of slope. The thalwegs of meltwater channels were
178 digitized as polylines and classified as either subglacial or lateral according to the criteria set out by
179 Greenwood *et al* (2007). All subglacial bedforms were mapped as polygons, including: subglacial ribs
180 (ribbed moraine), drumlins, mega-scale glacial lineations, and streamlined bedrock features. Our
181 mapping builds on earlier low-resolution mapping from Landsat and SPOT satellite imagery and field

182 surveys (Knight, 2003; Greenwood and Clark, 2009a), and has resulted in the creation of a
183 comprehensive database of Northern Irish eskers, consistent with the NextMap 5 m resolution data used
184 for the rest of the UK (Clark et al., 2018), and detailed mapping of glacial landforms in SW Northern
185 Ireland at 0.4 m resolution.

186 *3.2 Ground Penetrating Radar*

187 Ground Penetrating Radar (GPR) data were acquired in August and November 2016. A total of ~1.8
188 km are presented here, including profiles along the crestlines of the eskers and cross profiles in a range
189 of topographic contexts and for different esker forms. A 32-bit Mala Ground Explorer (GX) controller
190 unit connected directly to a 160MHz GX shielded antenna on a rough terrain skid plate was used in
191 August 2016. Radar profiles were acquired at a constant walking pace in a continuous, time-triggered
192 shot mode using hyperstacking to reduce random noise. A Mala Ramac system consisting of a 4 m-long
193 Rough Terrain Antenna, comprising in-line, unshielded transmitting and receiving antennas with a 1.5
194 m spacing and 100MHz centre frequency was used in November 2016. Collection of radar data was
195 performed at a constant walking pace, in a time-triggered mode, with 16 stacks at a delay of 0.5-seconds.
196 All radar survey lines were simultaneously mapped using a Leica CS15 differential Global Positioning
197 System (dGPS) unit to topographically correct the profiles.

198 Processing of radar data was performed within REFLEXW v7.5.9, the proprietary software of Karl
199 Sandmeier under licence number 401 provided to Queen's University, Belfast. A standard processing
200 sequence was developed, using the following steps: static correction of time-zero drift, removal of low
201 frequency signal saturation (dewow), application of gain to increase the visibility of reflections at depth,
202 diffraction stack migration, background removal to reduce antenna ringing, bandpass filtering and
203 topographic correction with the associated dGPS trace, finally radargrams were plotted in MatLab
204 v9.1.0.441655 (Neal, 2004; Cassidy and Jol, 2009). A velocity of 0.1 m/ns for migration was used,
205 consistent with exposures of eskers in sand extraction pits, hillside scars and road-cuts (see Section 3.3)
206 (Russell et al., 2001; Pellicer et al., 2012; Livingstone et al., 2016). GPR profiles were interpreted by
207 identifying high-amplitude reflectors indicative of bounding surfaces between radar facies. Six radar
208 facies (*sensu* Gawthorpe *et al.*, 1993) were differentiated based upon depositional characteristics,
209 including associations with sediment facies identified from exposures in the field and the broad
210 characteristics of reflectors within a unit (Table 1). Lateral discontinuities and offset reflectors were
211 interpreted as geological faults (e.g. Fiore et al., 2002).

212 *3.3 Sedimentology*

213 Gravel pit exposures adjacent to, and below, the GPR profiles were investigated to provide an insight
214 into the flow conditions responsible for ridge formation in the Evishanoran Esker, and to provide
215 ground-truthing for the interpretation of radargrams. Four sediment exposures were logged within the
216 complex, multi-ridge system and the simple, single-ridge system (Fig. 2). Scaled sediment logs were
217 drawn to record stratigraphic data, including details on the sedimentary structures, texture, and the unit

218 characteristics, such as bed geometry and contacts. Lithofacies were based on Evans and Benn (2004).
219 Clast macrofabric and palaeoflow indicators (e.g. ripples) supplemented stratigraphic logs (Miall,
220 1985).

221 **4.0 Results and interpretations**

222 *4.1 Glacial Geomorphology*

223 A complete map of the glacial meltwater landforms of Northern Ireland is presented in Figure 2a. The
224 map contains 457 esker ridges, totalling 220 km in length, compared to 63 esker ridges (40 km) detailed
225 for this region in the BRITICE v2 database (Clark *et al.*, 2018). Esker distribution is heterogeneous,
226 with the majority concentrated along a NE-SW axis to the south of the Sperrin Mountains and a > 20
227 km long N-S trending esker system to the north of the Lough Neagh Basin. Meltwater channels most
228 commonly occur near upland regions (Fig. 2a). Meltwater channels have been documented by previous
229 mapping efforts and are ubiquitous across Northern Ireland (Charlesworth, 1924; Colhoun, 1970;
230 Knight, 2006; Greenwood and Clark, 2009a).

231 We present a detailed map of the glacial geomorphology of SW Northern Ireland in Figure 2b, including
232 moraines, meltwater channels (lateral and subglacial), eskers and subglacial bedforms (lineations and
233 ribs). To the south of the Sperrin Mountains, a complex system of over 80 ridges form the Evishanoran
234 Esker system, spanning > 20 km and demonstrating considerable variation in morphology over its
235 length (Fig. 2 and 3). The esker system is oriented SW-NE, broadly aligned with an area of subglacial
236 ribs. Across this region, further glaciofluvial landforms associated with the esker system are observed.
237 Most notably, the SW sector is associated with a series of subglacial meltwater channels cut into a slope
238 that trends against the regional northwards ice flow, fan-shaped deposits at the northern terminus of
239 some eskers, and a kame terrace on the southern slopes of the Sperrin Mountains. To the SW, the esker
240 system in the Fintona Hills likely forms a meltwater routeway with the Evishanoran Esker that was
241 active during later stages of deglaciation (Knight, 2019). We define three distinct esker sections based
242 on variations in esker planform; the northern sector of the esker is composed of a predominantly simple
243 system of single ridges, the central sector is dominated by a complex, arborescent ridge network
244 distributed around a hill (~100m relief), and the southern sector comprises a complex, anabranching
245 system of multiple subparallel ridges (Figs. 3, 4).

246 In the northern sector of the esker system (Fig. 4a,b), a simple planform dominates, consisting of nine
247 consecutive ridges, with a total length of ~9 km (Table 2). The esker system trends uphill towards the
248 NE, with ridges orientated along a uniform, broad valley bottom. However, the eskers in this sector are
249 morphologically complex. Some consecutive ridges are offset, while others terminate in fan-shaped
250 deposits at their northern end, or exhibit enlargements in the esker profile (Fig. 4b; Table 2). These
251 ridges display considerable variability in size; ranging from 25 to 80 m in width and from 5 to 15 m in
252 relief. We identify a series of six small moraine ridges across this sector, which record former ice margin

253 standstills. Three of the four esker enlargements and fan-shaped deposits are observed coincident with
254 moraines.

255 Further SW (central sector), the esker transitions into a complex, arborescent system of short ridges
256 (~0.3 km long) with more subdued relief (~6 m). This coincides with a change to greater variability in
257 relief in the surrounding topography (183 – 296 m a.s.l.) and a broadly downhill trend towards the NE.
258 The southern end of the esker is split around a hill, with the western limb trending S-N before turning
259 W-E, where it is cross-cut by the eastern limb, which trends N-S (Figs. 2a, 4c). The esker ridges within
260 this sector display a simple morphology, with an enlargement only observed on a single ridge. We
261 mapped a single moraine within this esker sector, which coincided with the esker enlargement.

262 The southern sector consists of multiple, subparallel ridges along a slope, which broadly trends downhill
263 to the NE. While considerable variation in relief is observed due to the undulating terrain, cross-cutting
264 relationships are absent within this sector, although ridges are observed to bifurcate (Fig. 4d). A single
265 small esker enlargement is observed within this sector and a small moraine is present at the eastern end
266 of the system.

267 Complex geological faulting is observed across the study region (Fig. 2). Esker ridges commonly occur
268 near faults, while some also change orientation to follow faultlines (GSNI, 2016) (Fig. 2). This is
269 illustrated by the large fault system towards the S of the region, which trends ENE-WSW; a high
270 concentration of esker ridges within the southern sector of the esker display a spatial correspondence to
271 the fault and associated valley (Fig. 4d). This includes coincidence of individual ridges in the central
272 sector of the Evishanoran Esker with faults, where the main esker trends NE-SW (Fig. 2c). Further
273 examples of correspondence between geological faults and eskers are not limited to the Evishanoran
274 Esker: to the west a small series of eskers change orientation to follow a fault which trends NW-SE,
275 highlighted in Figure 2c. These changes occur three times over the ~ 5 km length of this esker.

276 *4.2 Esker Internal Architecture*

277 *4.2.1 Radar facies (RF) description and interpretation*

278 The GPR radar facies from both shielded 160MHz and unshielded 100MHz Rough Terrain antennas
279 were found to be broadly comparable (see below) and are outlined in Table 1. In this section we describe
280 facies characteristics in detail and interpret the depositional environments.

281 *4.2.1 RF1 – Coarse, poorly-bedded deposits*

282 RF1 often constitutes the core of the esker ridge, forming a tabular unit (up to 10 m thick) of
283 discontinuous, chaotic reflectors subparallel to the bed slope. The lower portion of RF1 often contains
284 hyperbola-generating point reflections. This unit is conformably overlain by RF2 or RF3, or truncated
285 by RF4 (Table 1).

286 Chaotic facies have been widely attributed to coarse, poorly-sorted deposits (Burke et al., 2008; Pellicer
287 and Gibson, 2011; Franke *et al.*, 2015; Livingstone et al., 2016; Perkins et al., 2016). This is supported
288 by sediment exposures through RF1, which comprise a variety of massive, coarse, gravelly or diamictic

289 deposits interpreted to have formed by the rapid deposition of hyperconcentrated flows (Fig. 5c; 5d)
290 (Saunderson, 1977; Gorrell and Shaw, 1991; Pellicer and Gibson, 2011; Pellicer et al., 2012;
291 Livingstone et al., 2016; Lang *et al.*, 2017). Previous studies consider point reflections to represent out-
292 of-plane boulder clusters and a coarsening of material within the ridge (Burke, 2010; Burke et al., 2012).
293 Out of plane reflections (sideswipes and hyperbola) are observed to be artefacts of upstanding surface
294 objects such as trees, poles and metal farm gates (Neal, 2004). These are most notable on data from the
295 100MHz unshielded antenna, and thus are disregarded in our interpretations.

296 4.2.2 RF2 – *Horizontally-bedded sands*

297 RF2 generally forms tabular units (~5 m thick) of continuous, subhorizontal reflectors (up to 30 m long)
298 that form parallel to the bed slope (<5° dip from horizontal). It typically forms a central unit in the esker
299 profile, regularly underlain by RF1 and overlain by RF3.

300 Previous studies have attributed similar patterns of subhorizontal reflectors to the vertical accretion of
301 finer material (Perkins et al., 2016). This interpretation is consistent with sediment exposures through
302 RF2 (Fig. 5a), which reveal horizontally-bedded sands and gravels, likely deposited in a lower flow
303 energy environment than RF1 (Banerjee and McDonald, 1975; Burke et al., 2012).

304 4.2.3 RF3 – *Delta foresets composed of sands and gravelly sand*

305 RF3 forms laterally constrained, wedge-shaped units (2 – 5 m thick) which unconformably overlie the
306 older esker deposits (Table 1). They comprise a series of onlapping, low-angle (4° - 15° from
307 horizontal), N to NE dipping reflections. RF3 is always the topmost unit where identified and therefore
308 represents the final stage of esker building.

309 We interpret the dipping reflectors as foreset beds deposited during lower energy flow conditions
310 compared to RF1 (Fiore et al., 2002; Burke et al., 2008, 2010). Foreset-backset macroforms in eskers
311 are indicative of deposition in a subglacial conduit widening during high-energy flows (Burke *et al.*,
312 2010). As we do not observe any backsets associated with the foreset deposits, deposition is likely not
313 within a subglacial conduit widening. A sediment exposure located NE of a radar survey within a ridge
314 dominated by RF3 (Fig. 9) documents a <1 m thick unit of gravelly-sand, cross-stratified and downflow-
315 dipping deposits (Fig. 5b). These foreset deposits are interpreted to have formed due to a change in
316 hydraulic conditions related to flow expansion (Fiore *et al.*, 2002; Winsemann *et al.*, 2007). We interpret
317 these deposits as either delta foresets deposited as water flowed from a subglacial conduit into a
318 proglacial lake, in some places forming shallow-water mouth-bars (Winsemann *et al.*, 2009; 2018; Lang
319 *et al.*, 2017), or subaqueous fan deposits (Winsemann *et al.*, 2009).

320 4.2.4 RF4 – *Concave, erosional trough-fills*

321 RF4 is defined by strong, concave-upwards bounding reflectors and subhorizontal to concave internal
322 reflectors (Table 1). The bounding reflectors vary in angle, with the units ranging from narrow, steep-
323 sided basins to broader infills, which may extend for up to 60 m along the esker surface and reach
324 thicknesses of up to 10 m. RF4 truncates underlying facies, displaying an erosional, lower bounding

325 surface. Most frequently, RF4 is located near the surface of the esker, but in places is conformably
326 overlain by RF3. RF4 is interpreted as erosional troughs, formed during the late-stages of esker genesis
327 as water incised into the underlying sediments, and subsequently filled as flow conditions waned
328 (Gorrell and Shaw, 1991; Sambrook-Smith et al., 2006; Perkins et al., 2016).

329 4.2.5 RF5 – Post-glacial infill

330 Present along the flanks in cross-profile surveys of esker ridges, RF5 is separated from the main esker
331 ridge elements by a strong bounding surface, which dips steeply away from the esker (Table 1). The
332 interior of these units is strongly attenuated and characterised by homogenous reflections, which are
333 broadly horizontal. RF5 is interpreted as postglacial infill of the area surrounding the esker ridge. The
334 reflection patterns are consistent with that of peat, which is prevalent across Ireland and confirmed by
335 observations in the field (Jol and Smith, 1991; Pellicer *et al.*, 2012).

336 4.3 Site architecture

337 At each site, radar profiles were divided into radar facies according to Table 1 and Section 4.2 above.
338 Here we describe the architecture of individual esker ridges and outline the processes responsible for
339 their formation.

340 4.3.1 Site 1

341 Site 1 is a 1.6 km long, broad, round-crested esker ridge at the northern termination of the single ridge
342 esker system (northern sector). We conducted a 0.9 km, 100 MHz radar survey along a road following
343 the crest of the esker ridge (Fig. 6). The ridge is situated along a forest-covered valley bottom on a slope
344 that dips towards the southwest and is significantly wider than southerly ridges within the system (up
345 to 140 m wide and 16 m high). The esker surface displays minor undulations (<1 m over ~ 90 m).

346 The architecture of the esker ridge is defined by a semi-continuous bounding surface with varying
347 elevation along the upper part of the radar profile (Fig. 6). Below this bounding surface is a core of RF1
348 present along the whole esker profile. The chaotic reflections suggest coarser material with a lack of
349 structure, so are interpreted to have formed by rapid deposition during high flow velocities (Burke *et*
350 *al.*, 2010; Pellicer and Gibson, 2011; Franke *et al.*, 2015; Livingstone *et al.*, 2016). At around 500 m
351 along the profile, side-swipes are observed, likely relating to signal scattering from surface obstacles
352 (Cassidy and Jol, 2009). No lower bounding surface is observed for this unit, but a maximum thickness
353 of 15 m is present at ~ 600 m. Towards the esker surface, the semi-continuous bounding surface defines
354 units of RF4 from 250 m onwards. The concave trough fills (RF4) vary in size, up to ~ 6 m deep and ~
355 80 m wide. At multiple locations the contact with RF4 and underlying reflectors is erosional (Fig. 6).
356 The reflectors observed in these concave infills are less chaotic, which we interpret to have formed as
357 erosional troughs infilled by finer sediment as flow energy waned (Sambrook-Smith *et al.*, 2006; Franke
358 *et al.*, 2015; Table 1). Trough-fill features observed in eskers have previously been interpreted to occur
359 when thermomechanical excavation is outweighed by creep closure, leading to increased flow velocities
360 and the erosion of underlying sediments (Perkins *et al.*, 2016).

361 4.3.2 Site 2

362 Fig. 7 shows a 0.6 km, 160 MHz radar profile taken along the crest of a 1.9 km long, round-crested
363 ridge, near the southern end of the simple esker system (northern sector). Fig. 8 displays a cross-profile
364 (including a short long-profile section of the crestline), taken from just over halfway along the ridge.
365 The topographic context of the system is largely uniform, with the ridge trending up a reverse bed slope
366 along the valley floor. The ridge morphology varies along its length. Undulations (up to 2 m high) are
367 observed to be associated with esker widening, and the ridge generally becomes smaller towards the
368 north (downflow), terminating in a fan-shaped deposit.

369 Two strong, horizontal bounding reflectors divide the ridge into three architectural units. These
370 bounding surfaces are discordant with the undulating esker surface. The lowest bounding surface is
371 observed at ~224 m elevation, with the underlying unit comprising a core of RF1 (present along the
372 length of the profile). Variations in thickness (~1 - 4 m) are observed, although no clear esker base is
373 identified. Between 0 - 10 m distance, a single unit of RF4 is present, cutting into RF1 with a depth of
374 ~1 m. This lower radar element relates to the initial stages of esker formation, and indicates high flow
375 energy and deposition of coarse material (Pellicer and Gibson, 2011; Livingstone *et al.*, 2016). Above
376 the bounding surface at ~224m elevation, the radar facies of the central unit varies spatially. Chaotic
377 reflections (RF1) dominate the upflow section from 400 – 550 m distance. Moving downflow, these
378 reflections become more continuous and in places exhibit a downflow dip (RF3; ~ 250m distance). The
379 change to more continuous reflectors indicates the deposition of better sorted material, perhaps due to
380 lower energy flow conditions. Above the upper bounding surface (225 m elevation), a ~2 m thick,
381 tabular unit of RF3 is continuous between 0 – 200 m distance, but absent from 200 – 400 m distance.
382 The presence of coherent downflow dipping reflectors (RF3) indicates a switch to lower flow energy
383 conditions in a progradational depositional environment. Within Figure 8, RF3 has a convex-up,
384 lenticular reflector pattern. This may represent laterally and vertically stacked, shallow-water delta
385 mouth-bar lobes deposited at the ice sheet margin where water from the subglacial conduit enters a
386 glacial lake (Winsemann *et al.*, 2018). However, we are cautious not to overinterpret this portion of the
387 radar survey due to the non-linear survey route. This unit unconformably overlies the esker core and
388 does not extend over the esker flanks, coinciding with an increase in esker height. This suggests that
389 deposition was constrained by ice walls (Fig. 8). Foreset-backset macroforms have been associated with
390 dynamic subglacial conduit enlargements during high flow energy conditions (Fiore *et al.*, 2002; Burke
391 *et al.*, 2010). The absence of backset deposits within this esker suggests another mechanism was
392 responsible for the change to progradational deposition.

393 Between 400 - 500 m distance, subhorizontal to chaotic reflections (RF1 and RF2) are observed along
394 the esker surface, coincident with an undulation and widening of the esker ridge. Overall, esker
395 architecture records a transition from hyperconcentrated flows during the initial stages, to lower energy
396 flow conditions and the deposition of delta foresets at the ice sheet margin. In cross-profile, up to 8 m

397 of post-glacial peat deposition (RF5) is documented on the esker flanks. This may result in less than
398 50% of the true esker height being observable at the surface (Jol and Smith, 1991; Pellicer et al., 2012).

399 4.3.3 Site 3

400 Figure 9 presents a 0.2 km, 160 MHz radar profile along the crest of a 0.8 km long round-topped esker
401 ridge, within the complex multi-ridge system (central sector). The ridge is situated in an area of steep,
402 hilly topography. At ~300 m along the esker morphology develops from a narrow ridge (~50 m wide)
403 into a broad, fan-shaped enlargement which is ~130 m wide and ~250 m long, before the ridge
404 terminates in a narrower section (~50 m wide) that is ~200 m long in an open topographic basin that
405 drains to the northwest. The radar profile starts on the summit of a hill at the beginning of the
406 enlargement and then follows the esker crest downslope (Fig 9). Three other ridges are located adjacent
407 to the studied esker, terminating in the same basin. A gravel pit is located at the terminus of the ridge,
408 consisting of a series of sand and gravel foreset units which dip to the northeast (Fig. 5b).

409 Within the lowest radar unit, between 0 – 40 m distance, the sequence is dominated by at least 3 m of
410 coherent horizontal reflections (RF2) indicating vertical accretion of fine material (Burke *et al.*, 2012).
411 Poor radar penetration prevents the identification of the lower bounding surface of this unit. From 120
412 – 170 m along flow, a unit up to 7 m thick, composed of more discontinuous reflections (RF1 and RF2),
413 represents a lateral transition to coarser material lacking structure, interpreted to be deposited
414 subglacially under higher flow energy (Pellicer and Gibson, 2011; Franke *et al.*, 2015; Livingstone *et*
415 *al.*, 2016). The upper section of the radar profiles is dominated by continuous, downflow-dipping
416 parallel reflectors which are convex-up lenticular perpendicular to flow. These units are typically quite
417 thin (up to ~2m) with low dip angles. From 0 – 140 m, there are two units of RF3 along the surface, but
418 140 m onwards is characterised by a single unit of RF3 along the surface. These upper units likely
419 represent a series of delta foresets and cross-stratified sands and gravels, deposited during lower energy
420 flow conditions in a progradational environment (Franke *et al.*, 2015). The thin beds and low dip angle
421 suggest deposition within a shallow water environment (Winsemann *et al.*, 2018). We interpret this
422 sequence of foresets, composed of cross-stratified sands and gravels, as shallow-water delta foresets
423 deposited on top of an esker, as meltwater exits the subglacial conduit at the ice sheet margin
424 (Winsemann *et al.*, 2007). The transition to a broader, fan-shaped morphology of the esker enlargement
425 associated with RF3 supports the interpretation that the delta foresets are superimposed on a core of
426 esker material that was deposited subglacially (Fig. 9).

427 4.3.4 Site 4

428 Figure 10 shows a 0.18 km long, 160 MHz radar profile along part of the crest of a 0.75 km long round-
429 crested esker within the complex, multi-ridge to anabranching esker system (southern sector). The esker
430 system is situated in an area of complex, hilly topography. The general esker trend is subparallel to a
431 fault-controlled valley, with ridges situated in and around it (Fig. 5d).

432 A single bounding surface is semi-continuous along the radar profile, present from 0 – 70 m distance,
433 at an elevation of ~ 233 m (Fig. 10). Below this bounding surface, a ~2 m thick core unit of chaotic
434 reflections (RF1) is present in sections of the radar profile where penetration was deep enough. These
435 chaotic reflections suggest the presence of coarse material deposited under high energy flow conditions
436 (Pellicer and Gibson, 2011; Livingstone *et al.*, 2016). Above the bounding surface, the radar units (~4
437 m thick) comprise more continuous reflections which are either subhorizontal or downflow dipping
438 (RF2 and RF3). This represents an increase in structure as finer material was deposited during lower
439 energy flow conditions (Franke *et al.*, 2015). The upflow section (0 - 80 m distance) is dominated by
440 RF1 and RF2, while the downflow section (80 m distance onwards) consists of more coherent units of
441 RF3. This transition to fine-grained foresets (RF3) coincides with a change to a downslope trend.

442 **5.0 Discussion**

443 The following section seeks to further our understanding of esker formation based on the sedimentary
444 architecture of a morphologically diverse esker system. First, the broad-scale architecture is considered
445 in order to develop a depositional model of esker formation. Second, local controls on esker formation
446 and morphology are discussed. Finally, we use our findings to reconstruct the ice sheet retreat pattern
447 and retreat rate for the Omagh Basin region.

448 5.1 Esker formation

449 5.1.1 A time-transgressive model of esker deposition

450 The Evishanoran Esker has a broadly homogeneous large-scale sedimentary architecture, despite
451 changes in esker morphology and topographic context (Figs. 6-10). GPR surveys reveal two main styles
452 of deposition during esker formation. Initial esker growth involved deposition of coarse gravel or
453 diamict from subglacial hyperconcentrated flows, which may have occurred in a somewhat synchronous
454 manner (Saunderson, 1977; Gorrell and Shaw, 1991; Pellicer and Gibson, 2011). Offset ridge
455 relationships and eskers terminating in subaqueous fans or deltas in the northern sector suggest that this
456 deposition likely extended for a maximum of a few kilometres up-ice, rather than tens of kilometres
457 (Fig. 4b). Later stages of esker growth coincide with a transition to well-sorted, deposits as flow energy
458 waned (Franke *et al.*, 2015). The sedimentary structures document a variety of hydrological processes
459 during the final stages of formation (RF2, RF3 and RF4), in contrast to the simple earlier event
460 dominated by hyperconcentrated flows (RF1).

461 As meltwater approaches the ice sheet margin, subglacial conduits experience reduced creep closure
462 (reaching zero at the ice margin: Rothlisberger, 1972). Despite this, thermomechanical excavation
463 continues to enlarge the subglacial conduit, meaning that the subglacial conduit grows towards the ice
464 sheet margin (Drews *et al.*, 2017). This expansion of the subglacial conduit is expected to cause a
465 progressive reduction in flow energy and carrying capacity (Hewitt and Creyts, 2019), resulting in
466 increased sedimentation rates (Beaud *et al.*, 2018) and the deposition of well-sorted, finer material. This
467 results in an enlargement of the esker profile at or near to former ice margin standstills (Fig. 11a). Flow

468 expansion due to conduit enlargement and subglacial meltwater drainage into the proglacial lake caused
469 a fall in flow energy and the formation of deltas/outwash fans (Winsemann *et al.*, 2007). In this situation,
470 the observed vertical upwards-sorting sequence is associated with decreasing flow energy as deposition
471 occurs progressively closer to the ice sheet margin during retreat (Walther, 1894).

472 Esker size, and the thickness of stratigraphic units, is dependent on the duration and rate of deposition.
473 As we described, the deposition rate is likely linked to the proximity of a location to the ice sheet
474 margin, as well as rates of sediment supply. The duration of deposition is related to the rate of ice sheet
475 margin retreat. Rapid margin retreat will reduce the time available for deposition, while a standstill will
476 result in enhanced deposition at and near the ice sheet margin. Therefore, we suggest that enlargements
477 in the esker profile could indicate former ice margin positions. For a stable ice sheet margin position,
478 we would expect a simple esker profile which grows in size towards its terminus. However, variations
479 in the retreat rate during deglaciation will lead to the superimposition of later esker deposits during
480 time-transgressive esker formation (Fig. 11b). We suggest the observed esker enlargements are a form
481 of esker bead deposited time-transgressively at the ice sheet margin (e.g. Livingstone *et al.*, 2020), and
482 superimposed on the core of subglacially deposited coarser material (Fig. 7, 9 and 11).

483 Enlargements in eskers or outwash fans/deltas are commonly observed across the Evishanoran Esker.
484 We suggest these enlargements can be used to reconstruct the relative rate of ice sheet margin retreat
485 and former ice margin positions. We favour formation of enlargements at the ice sheet margin, over the
486 possibility of formation within subglacial conduits, as we do not observe a backset-foreset macroform
487 diagnostic of this formation (Burke *et al.*, 2015). Caution must be taken when using these to reconstruct
488 the retreat rate, as variations in sediment supply may also influence the development of these
489 enlargements. But, the common co-occurrence of esker enlargements with topographic pinning points
490 (Fig. 4a) or moraines (Fig. 4b) supports an ice marginal origin.

491 Morphogenetic relationships have been proposed for eskers on the southern Fraser Plateau, British
492 Columbia (Burke *et al.*, 2015; Perkins *et al.*, 2016), while esker complexity has been related to
493 meltwater flow conditions and sediment supply in Svalbard and Iceland (Storrar *et al.*, 2015, 2020). In
494 central Northern Ireland, the relationship between esker morphology and the depositional processes is
495 less clear. At the local scale, undulations and enlargements of the esker profile appear to relate to a
496 time-transgressive depositional model during ice sheet retreat. An esker core is formed by synchronous
497 subglacial deposition, while enlargements are formed by the time-transgressive deposition of sediment
498 at or near to the ice sheet margin (Fig. 11).

499 5.1.2 Local controls

500 The morphology of eskers is influenced by the overall drainage characteristics during formation (Burke
501 *et al.*, 2015; Storrar *et al.*, 2015), as well as local factors (Clark and Walder, 1994; Storrar *et al.*, 2014a;
502 Knight, 2019). Beneath the Laurentide Ice Sheet, complex eskers and drainage routeways are more
503 common in areas of greater topographic variability (Storrar *et al.*, 2014a; Lewington *et al.*, 2020). In

504 the Evishanoran Esker, a similar relationship between complex esker morphology and topography is
505 observed. At the large-scale, the complex southern and central esker planforms are associated with a
506 topographic context dominated by high variations in relief, while the simpler northern sector is located
507 on the bottom of a broad valley floor. The distribution of eskers in the central sector clearly illustrates
508 this topographic influence, as eskers are deflected around the ~100m hill (Fig. 4c). We propose that
509 esker complexity in central Northern Ireland is largely controlled by the topographic variability.
510 Undulating topography may cause the subglacial conduit to fragment around obstacles or migrate as ice
511 thinned (Wright *et al.*, 2008; Storrar *et al.*, 2014b).

512 The complexity of esker systems in areas of high topographic variability reflects a combination of
513 spatial and temporal changes in the subglacial drainage network. Within the central sector of the
514 Evishanoran Esker, cross-cutting ridges suggest that the drainage system migrated during deglaciation
515 to create the complex esker network (Fig. 4c). In contrast, the anabranching nature of the southern
516 sector, with no cross-cutting relationships may instead represent a drainage network which is
517 fragmented by the complex topography (Fig. 4d). This is supported by the association with a series of
518 meltwater channels cut into, and ascending, the hill to the south of this sector (Fig. 2b), which may have
519 been active at similar times. Pressurised meltwater eroded the meltwater channels on the southern slopes
520 of the hill. Reductions in pressure on the downslope trend then led to the deposition of the esker system
521 (Livingstone *et al.*, 2016). It is also possible that increased deposition on the downslope trend may have
522 led to channel clogging and avulsion (Storrar *et al.*, 2015).

523 Substrate characteristics have been hypothesised to influence the formation and distribution of eskers.
524 For example, eskers are more common on resistant bedrock (Clark and Walder, 1994). Esker
525 morphology in north-central Ireland is controlled by a variety of substrate factors, including the
526 influence of pre-existing glacial features (Knight, 2019). The transition from sandstone and limestone
527 in the south to the variably metamorphosed crystalline granites and gabbros in the north does not appear
528 to influence esker distribution in the region south of the Sperrin Mountains. This is despite the
529 fundamental differences in bedrock structure at the crystal scale. However, a high level of spatial
530 correspondence between eskers and geological faults is observed (Fig. 2). This correspondence includes
531 eskers in the southern sector running sub-parallel to a large fault-controlled valley, and pronounced
532 changes in the orientation of eskers to trend along faults (Fig. 2). The valley orientation also likely plays
533 a role in controlling the esker distribution. However, esker distribution appears to be fault-controlled
534 across central Northern Ireland, including in locations where there is no clear topographic control.
535 Enhanced groundwater flow along zones of higher transmissivity (e.g. faults) may influence the
536 distribution of the subglacial drainage system (Boulton *et al.*, 2007a; 2007b; 2009).

537 The morphometry of eskers may relate to a combination of sediment and meltwater supply (Shreve,
538 1985; Storrar *et al.*, 2015), but caution must be taken when solely using geomorphological observations
539 to investigate the hydrological system of a palaeo-ice sheet. Radar surveys revealed substantial post-

540 glacial peat infilling around eskers, reducing their relative relief in the northern sector. The relative
541 relief of one esker is 5 m, but with up to 6 m of esker deposits hidden below the surface (Fig. 8).
542 Extensive peat deposits, up to 5.5 m thick, have been documented in the Irish Midlands (Pellicer and
543 Gibson, 2011; Pellicer *et al.*, 2012), which must be taken into consideration when using esker
544 dimensions to gain an insight into glacial history.

545 5.2 Implications for deglaciation of Northern Ireland

546 Three main ice dispersal centres operated during the deglaciation of the north of Ireland. This includes
547 an upland ice dispersal centre in the Donegal Mountains, and lowland ice domes in the Lough Neagh
548 and Omagh basins (Knight, 1997; Knight and McCabe, 1997; McCarron, 2013). Across this region,
549 meltwater landforms and small moraines record the final retreat pattern of the Irish Ice Sheet. Here we
550 describe the broader retreat patterns of the Irish Ice Sheet, before using the Evishanoran Esker to
551 describe the retreat rate of the Omagh Basin ice.

552 The Donegal Mountains, Lough Neagh and Omagh ice domes were coalescent at the start of
553 deglaciation, indicated by subglacial bedform patterns (Fig. 2a), but became isolated ice domes
554 following ice sheet thinning (Fig. 2a and 2b). Eskers oriented radially around the Lough Neagh basin
555 record the final pattern of retreat. Lough Neagh ice separated from the Lough Erne/Omagh Basin Ice
556 Dome along an approximately N-S axis located to the south of the eastern Sperrin Mountains (Fig. 2a).
557 In the west, the Lough Erne Ice Dome separated from ice sourced from the Donegal and Sligo
558 Mountains sometime between 15-16ka, according to the isochrons of Wilson *et al.* (2019). Lateral
559 meltwater channels record the downwasting of ice flowing from Sligo and Donegal into the Lough Erne
560 Basin, indicating when summits became ice-free and the separation of these ice dispersal centres (Fig.
561 2b). The position of these channels suggests that Donegal ice persisted long enough to flow into a mostly
562 deglaciated Lough Erne Basin (Fig. 2b). This is consistent with dating evidence indicating that the
563 Donegal Mountains held the final remnants of the British-Irish Ice Sheet in Ireland (Wilson *et al.*, 2019).
564 The relative retreat rate and former ice margin standstills can be identified from the morphology of the
565 Evishanoran Esker and associated landforms. The initial southwards ice margin retreat from the Sperrin
566 Mountains was quite slow across the northern esker sector. We identify at least four former ice margin
567 standstills over the 9.3 km this sector spans, from evidence of five small moraines, two esker
568 enlargements, three delta/outwash fan deposits and sedimentological information (Fig. 2b,c). These
569 former standstill locations are mostly located at topographic pinning points. The retreat rate was more
570 rapid across the central sector. A single moraine and fan-shaped deposit at the northern end of this sector
571 suggest only one standstill across the 7.4 km sector length. The retreat rate across the southern sector
572 may have slowed slightly, as the retreat direction became oriented towards the SW. Geomorphological
573 evidence suggests one or two possible standstills over a distance of 6.5 km. A small moraine at the
574 north-eastern side of the sector suggests a standstill at the start of esker formation in this sector, where
575 a hill (~150m relative relief) may have acted as a pinning point. A small enlargement associated with

576 foreset deposits may have formed under a short-lived standstill in the centre of this sector (Fig. 10).
577 However, the retreat was likely more rapid than in the northern sector due to the relative lack of
578 geomorphological evidence. Continued retreat to the SW of our study area led to the formation of eskers
579 and meltwater channels throughout the Lough Erne Basin and Fintona Hills (Knight, 2003; 2019).

580 **6.0 Conclusions**

581 The Evishanoran Esker was deposited time-transgressively in a subglacial, closed conduit or at the ice
582 sheet margin and records the final stages of ice retreat in this region from the Sperrin Mountains to the
583 south. Esker distribution is a result of the dynamic evolution of the subglacial hydrological system, and
584 does not record an extensive drainage network. Based on our observations, we present a series of key
585 points regarding the deglacial history and broader implications for esker formation:

- 586 1. The Evishanoran Esker was formed by two main styles of deposition that occurred repeatedly
587 during deglaciation. An initial event of hyperconcentrated flows within the subglacial conduit
588 deposited the poorly sorted, coarse sediment that forms the esker core. This subglacial
589 deposition likely occurred in a semi-synchronous manner. This was followed by the deposition
590 of delta foresets composed of well-sorted material, superimposed on the subglacially deposited
591 esker core. These delta foresets were deposited time-transgressively at or near the ice sheet
592 margin due to flow expansion as subglacial meltwater entered a proglacial lake. Esker
593 enlargements occur where these time-transgressive delta deposits are observed, and likely
594 indicate former ice margin positions.
- 595 2. The internal architecture of eskers is broadly homogenous across all sectors, suggesting that
596 hydrological conditions are largely comparable. Variations in esker morphology cannot solely
597 be attributed to variations in drainage characteristics. Instead, we suggest local topographic
598 conditions influence esker complexity.
- 599 3. Using evidence for former ice margin standstills we reconstruct the variations in the retreat rate
600 across the Evishanoran Esker. Ice margin retreat across the northern sector was slow, with
601 retreat rate increasing during margin retreat across the central and southern sectors.
- 602 4. Geologic and topographic settings control esker distribution and formation. The close
603 association between the orientation and distribution of eskers and faults suggest that underlying
604 geological structural weaknesses act as a zone of high meltwater transmissivity. The
605 reconstruction of ice dynamics from meltwater features must also consider the influence of
606 local factors on distribution.
- 607 5. Post-depositional processes can have a significant influence on esker geomorphology. Post-
608 glacial fluvial erosion has previously been invoked to explain the fragmentation of some esker
609 systems. We identify significant post-glacial peat infilling which masks esker dimensions and
610 poses a problem for esker studies that rely solely on remote sensing morphometric analysis.

611

612 **Acknowledgements:**

613 We thank Mike Langton of GuideLineGeo (MALA) for the loan of radar equipment and advice. Digital
614 resources were made available under MOU205, courtesy of Land and Property Services, Northern
615 Ireland, supplied to Queen's University, Belfast. This study would also not be possible without the
616 generous access to land granted by multiple landowners in Northern Ireland. We kindly thank two
617 anonymous reviewers for their comments on this manuscript.

618

619 **Funding sources:**

620 This research did not receive any specific grant from funding agencies in the public, commercial, or
621 not-for-profit sectors.

622

623 **References:**

624 Alley, R.B., Blankenship, D.D., Bentley, C.R. and Rooney, S.T. (1986) Deformation of till beneath
625 ice stream B, West Antarctica. *Nature*, 322, 57-59.

626 Aylsworth, J.M. and Shilts, W.W. (1989) Bedforms of the Keewatin ice sheet, Canada. *Sedimentary
627 Geology*, 62(2-4): 407-428

628 Banerjee, I. and McDonald, B.C. (1975) Nature of esker sedimentation, in Jopling, A. V., and
629 McDonald, B. C., eds., *Glaciofluvial and glaciolacustrine sedimentation*: Society of
630 Economic Paleontologists and Mineralogists Special Publication No. 23: 132-154.

631 Bartholomew, I., Nienow, P., Mair, D., Hubbard, A., King, M.A. and Sole, A. (2010). Seasonal
632 evolution of subglacial drainage and acceleration in a Greenland outlet glacier. *Nature
633 Geoscience*, 3(6), 408-411.

634 Beaud, F., Flowers, G.E. and Venditti, J.G. (2018) Modeling Sediment Transport in Ice-Walled
635 Subglacial Channels and Its Implications for Esker Formation and Proglacial Sediment
636 Yields. *Journal of Geophysical Research: Earth Surface*, 123(12): 3206-3227

637 Bell, R.E., Studinger, M., Shuman, C.A., Fahnestock, M.A. and Joughin, I. (2007). Large subglacial
638 lakes in East Antarctica at the onset of fast-flowing ice streams. *Nature*, 445(7130), 904-
639 907.

640 Boulton, G.S., Hagdorn, M., Maillot, P.B. and Zatsepin, S. (2009) Drainage beneath ice sheets:
641 groundwater–channel coupling, and the origin of esker systems from former ice
642 sheets. *Quaternary Science Reviews*, 28(7-8), 621-638

- 643 Boulton, G.S., Lunn, R., Vidstrand, P. and Zatsepin, S. (2007b) Subglacial drainage by
644 groundwater–channel coupling, and the origin of esker systems: part II—theory and
645 simulation of a modern system. *Quaternary Science Reviews*, 26(7-8), 1091-1105
- 646 Boulton, G.S., Lunn, R., Vidstrand, P. and Zatsepin, S., (2007a) Subglacial drainage by
647 groundwater-channel coupling, and the origin of esker systems: part 1—glaciological
648 observations. *Quaternary Science Reviews*, 26(7-8), 1067-1090
- 649 Bradwell, T., Stoker, M.S., Golledge, N.R., Wilson, C.K., Merritt, J.W., Long, D., Everest, J.D.,
650 Hestvik, O.B., Stevenson, A.G., Hubbard, A.L. and Finlayson, A.G. (2008) The northern
651 sector of the last British Ice Sheet: maximum extent and demise. *Earth-Science*
652 *Reviews*, 88(3-4): 207-226
- 653 Brennand, T. A. (1994). Macroforms, large bedforms and rhythmic sedimentary sequences in
654 subglacial eskers, south-central Ontario: implications for esker genesis and meltwater
655 regime. *Sedimentary Geology*, 91(1–4), 9–55. [https://doi.org/10.1016/0037-0738\(94\)90122-](https://doi.org/10.1016/0037-0738(94)90122-8)
656 [8](https://doi.org/10.1016/0037-0738(94)90122-8)
- 657 Brennand, T.A. (2000) Deglacial meltwater drainage and glaciodynamics: inferences from
658 Laurentide eskers, Canada. *Geomorphology*, 32(3-4): 263-293
- 659 Budd, W.F., Keage, P.L. and Blundy, N.A (1979). Empirical studies of ice sliding. *Journal of*
660 *Glaciology*, 23, 157-170.
- 661 Burke, M. J., Brennand, T. A., & Sjogren, D. B. (2015). The role of sediment supply in esker
662 formation and ice tunnel evolution. *Quaternary Science Reviews*, 115, 50–77.
663 <https://doi.org/10.1016/j.quascirev.2015.02.017>
- 664 Burke, M. J., Woodward, J., Russell, A. J., Fleisher, P. J., & Bailey, P. K. (2008). Controls on the
665 sedimentary architecture of a single event englacial esker: Skeiðarárjökull, Iceland.
666 *Quaternary Science Reviews*, 27(19–20): 1829–1847.
667 <https://doi.org/10.1016/j.quascirev.2008.06.012>
- 668 Burke, M. J., Woodward, J., Russell, A. J., Fleisher, P. J., & Bailey, P. K. (2010). The sedimentary
669 architecture of outburst flood eskers: A comparison of ground-penetrating radar data from
670 Bering Glacier, Alaska and Skeiðarárjökull, Iceland. *Bulletin of the Geological Society of*
671 *America*, 122(9–10): 1637–1645. <https://doi.org/10.1130/B30008.1>

- 672 Burke, M.J., Brennand, T.A. and Perkins, A.J. (2012) Transient subglacial hydrology of a thin ice
673 sheet: insights from the Chasm esker, British Columbia, Canada. *Quaternary Science*
674 *Reviews*, 58: 30-55.
- 675 Callard, S.L., Cofaigh, C.Ó., Benetti, S., Chiverrell, R.C., Van Landeghem, K.J., Saher, M.H.,
676 Livingstone, S.J., Clark, C.D., Small, D., Fabel, D. and Moreton, S.G. (2020) Oscillating
677 retreat of the last British-Irish Ice Sheet on the continental shelf offshore Galway Bay,
678 western Ireland. *Marine Geology*, 420: 106087.
- 679 Cassidy, N.J. and Jol, H.M. (2009) Ground penetrating radar data processing, modelling and
680 analysis. *Ground penetrating radar: theory and applications*: 141-176
- 681 Charlesworth, J.K. (1926) The Evishnoran “Esker”, Tyrone. *Geological Magazine*, 63(5), 223-225.
682 doi:10.1017/S0016756800084156
- 683 Charlesworth, J.K. (1924). The glacial geology of the north-west of Ireland. *Proceedings of the*
684 *Royal Irish Academy*, 36b: 174-314
- 685 Chew, D.M., Flowerdew, M.J., Page, L.M., Crowley, Q.G., Daly, J.S., Cooper, M. and Whitehouse,
686 M.J. (2008) The tectonothermal evolution and provenance of the Tyrone Central Inlier,
687 Ireland: Grampian imbrication of an outboard Laurentian microcontinent?. *Journal of the*
688 *Geological Society*, 165(3): 675-685
- 689 Chiverrell, R.C., Thomas, G.S.P., Burke, M., Medialdea, A., Smedley, R., Bateman, M., Clark, C.,
690 Duller, G.A., Fabel, D., Jenkins, G. and Ou, X. (2020) The evolution of the terrestrial-
691 terminating Irish Sea glacier during the last glaciation. *Journal of Quaternary Science*,
692 doi:10.1002/jqs.3229
- 693 Clark, C.D. and Meehan, R.T. (2001) Subglacial bedform geomorphology of the Irish Ice Sheet
694 reveals major configuration changes during growth and decay. *Journal of Quaternary*
695 *Science: Published for the Quaternary Research Association*, 16(5): 483-496
- 696 Clark, C.D., Ely, J.C., Greenwood, S.L., Hughes, A.L., Meehan, R., Barr, I.D., Bateman, M.D.,
697 Bradwell, T., Doole, J., Evans, D.J. and Jordan, C.J. (2018) BRITICE Glacial Map, version
698 2: a map and GIS database of glacial landforms of the last British–Irish Ice
699 Sheet. *Boreas*, 47(1): 11
- 700 Clark, C.D., Hughes, A.L., Greenwood, S.L., Jordan, C. and Sejrup, H.P. (2012) Pattern and timing
701 of retreat of the last British-Irish Ice Sheet. *Quaternary Science Reviews*, 44: 112-146

- 702 Clark, P. U., & Walder, J. S. (1994). Subglacial drainage, eskers, and deforming beds beneath the
703 Laurentide and Eurasian ice sheets. *Geological Society of America Bulletin*, 106(2), 304–
704 314. [https://doi.org/10.1130/0016-7606\(1994\)106<0304:SDEADB>2.3.CO;2](https://doi.org/10.1130/0016-7606(1994)106<0304:SDEADB>2.3.CO;2)
- 705 Colhoun, A. (1971) The glacial stratigraphy of the Sperrin Mountains and its relation to the glacial
706 stratigraphy of north-west Ireland. *Proceedings of the Royal Irish Academy* 71B: 37–52
- 707 Colhoun, E.A. (1970). On the nature of the glaciations and final deglaciation of the Sperrin
708 Mountains and adjacent areas in the north of Ireland. *Irish Geography*, 6(2), 162-185.
- 709 Cummings, D.I., Kjarsgaard, B.A., Russell, H.A. and Sharpe, D.R. (2011) Eskers as mineral
710 exploration tools. *Earth-science reviews*, 109(1-2): 32-43
- 711 Dardis, G.F. (1986) Late Pleistocene glacial lakes in south-central Ulster, Northern Ireland. *Irish*
712 *journal of earth sciences*: 133-144
- 713 Davison, B.J., Sole, A.J., Livingstone, S.J., Cowton, T.R. and Nienow, P.W. (2019) The influence of
714 hydrology on the dynamics of land-terminating sectors of the Greenland Ice Sheet. *Frontiers*
715 *in Earth Science*, 7.
- 716 Delaney, C. (2001a) Esker formation and the nature of deglaciation: the Ballymahon esker, Central
717 Ireland. *North West Geography*, 1(2): 23-33
- 718 Delaney, C. (2001b) Morphology and sedimentology of the Rooskagh esker, Co. Roscommon. *Irish*
719 *Journal of Earth Sciences*: 5-22
- 720 Delaney, C. (2002) Sedimentology of a glaciofluvial landsystem, Lough Ree area, Central Ireland:
721 implications for ice margin characteristics during Devensian deglaciation. *Sedimentary*
722 *Geology*, 149(1-3): 111-126
- 723 Delaney, C.A., McCarron, S. and Davis, S. (2018). Irish Ice Sheet dynamics during deglaciation of
724 the central Irish Midlands: Evidence of ice streaming and surging from airborne LiDAR.
725 *Geomorphology*, 306, 235-253.
- 726 Drews, R., Pattyn, F., Hewitt, I.J., Ng, F.S.L., Berger, S., Matsuoka, K., Helm, V., Bergeot, N.,
727 Favier, L. and Neckel, N. (2017) Actively evolving subglacial conduits and eskers initiate
728 ice shelf channels at an Antarctic grounding line. *Nature communications*, 8: 15228
- 729 Dyke, A. and Prest, V. (1987) Late Wisconsinan and Holocene history of the Laurentide ice
730 sheet. *Géographie physique et Quaternaire*, 41(2): 237-263.

- 731 Evans, D. J. A., & Benn, D. I. (2004) A practical guide to the study of glacial sediments. Edward
732 Arnold, London.
- 733 Fiore, J., Pugin, A. and Beres, M. (2002) Sedimentological and GPR studies of subglacial deposits
734 in the Joux Valley (Vaud, Switzerland): backset accretion in an esker followed by an erosive
735 jökulhlaup. *Géographie physique et Quaternaire*, 56(1): 19-32
- 736 Fitzsimons, S.J. (1991) Supraglacial eskers in Antarctica. *Geomorphology*, 4(3-4): 293-299
- 737 Flint, R.F. (1930) The Origin of the Irish" Eskers". *Geographical Review*, 20(4): 615-630
- 738 Franke, D., Hornung, J. and Hinderer, M. (2015) A combined study of radar facies, lithofacies and
739 three-dimensional architecture of an alpine alluvial fan (Illgraben fan,
740 Switzerland). *Sedimentology*, 62(1): 57-86
- 741 Gawthorpe, R.L., Collier, R.L., Alexander, J., Bridge, J.S. and Leeder, M.R. (1993) Ground
742 penetrating radar: application to sandbody geometry and heterogeneity studies. *Geological*
743 *Society, London, Special Publications*, 73(1): 421-432
- 744 Geological Survey Northern Ireland (2016) Digital Geological Map of Northern Ireland – 10k. 10k
745 geology reproduced with the permission of the Geological Survey of Northern Ireland.
746 Crown Copyright 2018.
- 747 Gorrell, G. and Shaw, J. (1991) Deposition in an esker, bead and fan complex, Lanark, Ontario,
748 Canada. *Sedimentary Geology*, 72(3-4): 285-314
- 749 Greenwood, S. L., & Clark, C. D. (2009a). Reconstructing the last Irish Ice Sheet 1: changing flow
750 geometries and ice flow dynamics deciphered from the glacial landform record. *Quaternary*
751 *Science Reviews*, 28(27–28), 3085–3100. <https://doi.org/10.1016/j.quascirev.2009.09.008>
- 752 Greenwood, S. L., & Clark, C. D. (2009b). Reconstructing the last Irish Ice Sheet 2: a
753 geomorphologically-driven model of ice sheet growth, retreat and dynamics. *Quaternary*
754 *Science Reviews*, 28(27–28), 3101–3123. <https://doi.org/10.1016/j.quascirev.2009.09.014>
- 755 Greenwood, S.L., Clark, C.D. and Hughes, A.L. (2007) Formalising an inversion methodology for
756 reconstructing ice-sheet retreat patterns from meltwater channels: application to the British
757 Ice Sheet. *Journal of Quaternary Science: Published for the Quaternary Research*
758 *Association*, 22(6): 637-645

- 759 Greenwood, S.L., Clason, C.C., Helanow, C. and Margold, M. (2016) Theoretical, contemporary
760 observational and palaeo-perspectives on ice sheet hydrology: processes and
761 products. *Earth-Science Reviews*, 155: 1-27
- 762 Gregory, J.W. (1912) The relations of kames and eskers. *The Geographical Journal*, 40(2): 169-175.
- 763 Gregory, J.W. (1921) IV.—The Irish eskers. *Phil. Trans. R. Soc. Lond. B*, 210(372-381): 115-151.
- 764 Gregory, J.W. (1925) The Evishanoran Esker, 1 Tyrone. *Geological Magazine*, 62(10): 451-458.
- 765 Gregory, J.W. (1926) The Evishnoran “Esker”. *Geological Magazine*, 62(7): 336-336.
766 doi:10.1017/S0016756800084557
- 767 Gustavson, T.C. and Boothroyd, J.C. (1987) A depositional model for outwash, sediment sources,
768 and hydrologic characteristics, Malaspina Glacier, Alaska: A modern analog of the
769 southeastern margin of the Laurentide Ice Sheet. *Geological Society of America*
770 *Bulletin*, 99(2): 187-200.
- 771 Hebrand, M. and Åmark, M. (1989) Esker formation and glacier dynamics in eastern Skane and
772 adjacent areas, southern Sweden. *Boreas*, 18(1): 67-81.
- 773 Hewitt, I.J. and Creyts, T.T. (2019) A model for the formation of eskers. *Geophysical Research*
774 *Letters*, 46(12), pp.6673-6680.
- 775 Hinch, J. (1921) The eskers of Ireland. *The Irish Naturalist*, 30(12): 137-142
- 776 Hubbard, B. & Nienow, P. (1997) Alpine subglacial hydrology. *Quaternary Science Reviews*, 16,
777 939-955.
- 778 Iken, A., Bindschadler, R.A. (1986) Combined measurements of subglacial water pressure and
779 surface velocity of Findelengletscher, Switzerland: conclusions about drainage system and
780 sliding mechanism. *Journal of Glaciology*, 32(110): 101-119.
- 781 Jol, H.M. and Smith, D.G. (1991) Ground penetrating radar of northern lacustrine deltas. *Canadian*
782 *Journal of Earth Sciences*, 28(12): 1939-1947
- 783 Knight, J. (1997). Morphological and morphometric analysis of drumlin bedforms in the Omagh
784 Basin, north central Ireland. *Geografiska Annaler*, 79A: 255-266.
- 785 Knight, J. (1999). Geological evidence for neotectonic activity during deglaciation of the southern
786 Sperrin Mountains, Northern Ireland. *Journal of Quaternary Science*, 14(1): 45-57.

787 Knight, J. (2002). Bedform patterns, subglacial meltwater events, and Late Devensian ice sheet
788 dynamics in north-central Ireland. *Global and Planetary Change*, 35(3–4): 237–253.

789 Knight, J. (2003) Geomorphic evidence for patterns of late Midlandian ice advance and retreat in the
790 Omagh Basin. *Irish Geography*, 36(1): 1-22

791 Knight, J. (2006) Geomorphic evidence for active and inactive phases of Late Devensian ice in
792 north-central Ireland. *Geomorphology*, 75(1-2): 4-19

793 Knight, J. (2019) The geomorphology and sedimentology of eskers in north-Central
794 Ireland. *Sedimentary Geology*, 382: 1-24.

795 Knight, J. and McCabe, A.M. (1997) Identification and significance of ice-flow-transverse
796 subglacial ridges (Rogen moraines) in northern central Ireland. *Journal of Quaternary
797 Science*, 12(6): 519-524

798 Knight, J., Coxon, P., McCabe, A.M. and McCarron, S.G. (2004) Pleistocene glaciations in Ireland.
799 In *Developments in Quaternary Sciences*, 2: 183 – 191. Elsevier.

800 Lang, J., Sievers, J., Loewer, M., Igel, J. and Winsemann, J. (2017) 3D architecture of cyclic-step
801 and antidune deposits in glacial subaqueous fan and delta settings: Integrating outcrop
802 and ground-penetrating radar data. *Sedimentary Geology*, 362: 83-100

803 Lewington, E.L., Livingstone, S.J., Clark, C.D., Sole, A.J. and Storrar, R.D. (2020) A model for
804 interaction between conduits and surrounding hydraulically connected distributed drainage
805 based on geomorphological evidence from Keewatin, Canada. *The Cryosphere*, 14(9): 2949-
806 2976.

807 Livingstone, S. J., Utting, D. J., Ruffell, A., Clark, C. D., Pawley, S., Atkinson, N., & Fowler, A. C.
808 (2016). Discovery of relict subglacial lakes and their geometry and mechanism of drainage.
809 *Nature Communications*, 7. <https://doi.org/10.1038/ncomms11767>

810 Livingstone, S.J., Lewington, E.L., Clark, C.D., Storrar, R.D., Sole, A.J., McMartin, I., Dewald, N.
811 and Ng, F. (2020) A quasi-annual record of time-transgressive esker formation: implications
812 for ice-sheet reconstruction and subglacial hydrology. *The Cryosphere*, 14(6): 1989-2004

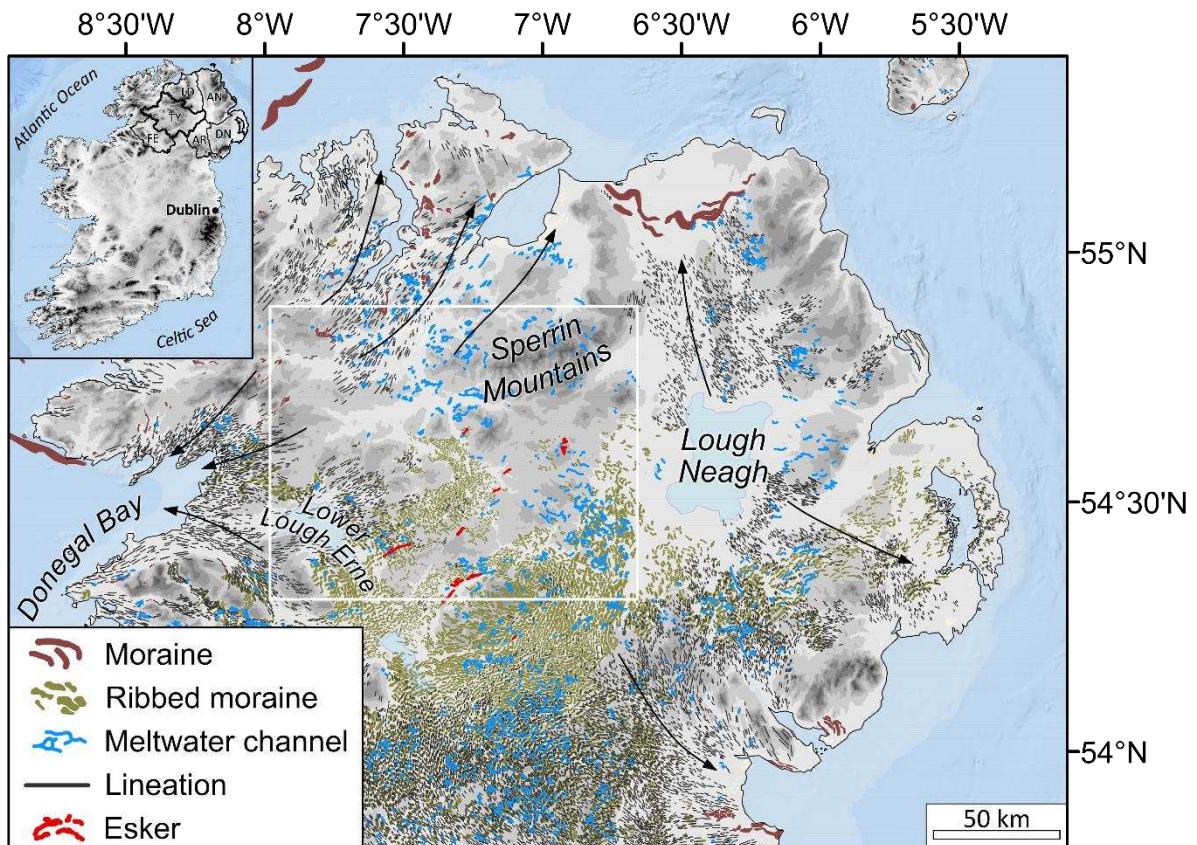
813 Livingstone, S.J., Storrar, R.D., Hillier, J.K., Stokes, C.R., Clark, C.D. and Tarasov, L. (2015) An
814 ice-sheet scale comparison of eskers with modelled subglacial drainage
815 routes. *Geomorphology*, 246: 104-112

- 816 Mäkinen, J. (2003) Time-transgressive deposits of repeated depositional sequences within
817 interlobate glaciofluvial (esker) sediments in Köyliö, SW Finland. *Sedimentology*, 50(2):
818 327-360
- 819 Margold, M., Jansson, K.N., Kleman, J., Stroeven, A.P. and Clague, J.J. (2013) Retreat pattern of
820 the Cordilleran Ice Sheet in central British Columbia at the end of the last glaciation
821 reconstructed from glacial meltwater landforms. *Boreas*, 42(4): 830-847
- 822 McCarron, S. (2013) Deglaciation of the Dungiven Basin, North-West Ireland. *Irish Journal of*
823 *Earth Sciences*, 31: 43-71
- 824 Miall, A.D. (1985) Architectural-element analysis: a new method of facies analysis applied to fluvial
825 deposits. *Earth Sci. Rev.*, 22: 261–308
- 826 Neal, A. (2004) Ground-penetrating radar and its use in sedimentology: principles, problems and
827 progress. *Earth-science reviews*, 66(3-4): 261-330
- 828 Ó Cofaigh, C., Evans, D.J.A. (2007) Radiocarbon constraints on the age of the maximum advance of
829 the British-Irish Ice Sheet in the Celtic Sea. *Quaternary Science Reviews* 26 (9–10), 1197–
830 1203
- 831 Ó Cofaigh, C., Weilbach, K., Lloyd, J.M., Benetti, S., Callard, S.L., Purcell, C., Chiverrell, R.C.,
832 Dunlop, P., Saher, M., Livingstone, S.J. and Van Landeghem, K.J. (2019) Early deglaciation
833 of the British-Irish Ice Sheet on the Atlantic shelf northwest of Ireland driven by
834 glacioisostatic depression and high relative sea level. *Quaternary Science Reviews*, 208: 76-
835 96
- 836 Pellicer, X. M., & Gibson, P. (2011). Electrical resistivity and Ground Penetrating Radar for the
837 characterisation of the internal architecture of Quaternary sediments in the Midlands of
838 Ireland. *Journal of Applied Geophysics*, 75(4), 638–647.
839 <https://doi.org/10.1016/j.jappgeo.2011.09.019>
- 840 Pellicer, X. M., Warren, W. P., Gibson, P., & Linares, R. (2012). Construction of an evolutionary
841 deglaciation model for the Irish midlands based on the integration of morphostratigraphic
842 and geophysical data analyses. *Journal of Quaternary Science*, 27(8), 807–818.
843 <https://doi.org/10.1002/jqs.2570>
- 844 Perkins, A. J., Brennand, T. A., & Burke, M. J. (2016). Towards a morphogenetic classification of
845 eskers: Implications for modelling ice sheet hydrology. *Quaternary Science Reviews*, 134:
846 19–38. <https://doi.org/10.1016/j.quascirev.2015.12.015>

- 847 Perkins, A.J., Brennand, T.A. and Burke, M.J. (2013) Genesis of an esker-like ridge over the
848 southern Fraser Plateau, British Columbia: Implications for paleo-ice sheet reconstruction
849 based on geomorphic inversion. *Geomorphology*, 190: 27-39
- 850 Price, R.J. (1969) Moraines, sandar, kames and eskers near Breidamerkurjökull,
851 Iceland. *Transactions of the Institute of British Geographers*: 17-43
- 852 Roberts, M.C., Niller, H.P. and Helmstetter, N. (2003) Sedimentary architecture and radar facies of a
853 fan delta, Cypress Creek, West Vancouver, British Columbia. *Geological Society, London,*
854 *Special Publications*, 211(1): 111-126
- 855 Röthlisberger, H. (1972) Water pressure in intra-and subglacial channels. *Journal of*
856 *Glaciology*, 11(62): 177-203
- 857 Russell, A.J., Knudsen, O., Fay, H., Marren, P.M., Heinz, J. and Tronicke, J. (2001) Morphology
858 and sedimentology of a giant supraglacial, ice-walled, jökulhlaup channel, Skeiðarárjökull,
859 Iceland: implications for esker genesis. *Global and Planetary Change*, 28(1-4): 193-216
- 860 Sambrook-Smith, G.H., Ashworth, P.J., Best, J.L., Woodward, J. and Simpson, C.J. (2006) The
861 sedimentology and alluvial architecture of the sandy braided South Saskatchewan River,
862 Canada. *Sedimentology*, 53(2): 413-434
- 863 Saunderson, H.C. (1977) The sliding bed facies in esker sands and gravels: a criterion for full-pipe
864 (tunnel) flow? *Sedimentology*, 24(5):623-638
- 865 Schoof, C. (2010) Ice-sheet acceleration driven by melt supply variability. *Nature*, 468(7325): 803
- 866 Shreve, R. L. (1985). Esker characteristics in terms of glacier physics, Katahdin esker system,
867 Maine. *Geological Society of America Bulletin*, 96(5), 639–646.
868 [https://doi.org/10.1130/0016-7606\(1985\)96<639:ECITOG>2.0.CO;2](https://doi.org/10.1130/0016-7606(1985)96<639:ECITOG>2.0.CO;2)
- 869 Smith, M.J. and Knight, J. (2011) Palaeoglaciology of the last Irish Ice Sheet reconstructed from
870 striae evidence. *Quaternary Science Reviews*, 30(1-2): 147-160
- 871 Sollas, W.J. (1896) A map to show the Distribution of Eskers in Ireland. *Sci. Trans. R. Dublin Soc*,
872 2(5): 785-822.
- 873 Stearns, L.A., Smith, B.E. and Hamilton, G.S. (2008). Increased flow speed on a large East
874 Antarctic outlet glacier caused by subglacial floods. *Nature Geoscience*, 1(12), 827-831.

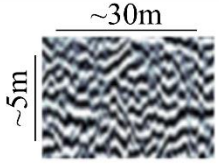
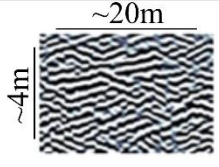
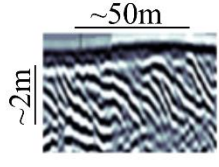
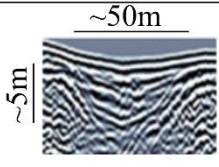
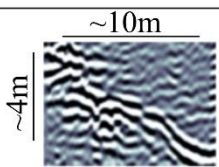
- 875 Storrar, R. D., Evans, D. J. A., Stokes, C. R., & Ewertowski, M. (2015). Controls on the location,
876 morphology and evolution of complex esker systems at decadal timescales,
877 Breidamerkurjökull, southeast Iceland. *Earth Surface Processes and Landforms*, 40(11),
878 1421–1438. <https://doi.org/10.1002/esp.3725>
- 879 Storrar, R.D., Ewertowski, M., Tomczyk, A.M., Barr, I.D., Livingstone, S.J., Ruffell, A., Stoker,
880 B.J. and Evans, D.J. (2020) Equifinality and preservation potential of complex
881 eskers. *Boreas*, 49(1), 211-231.
- 882 Storrar, R.D., Stokes, C.R. and Evans, D.J. (2013) A map of large Canadian eskers from Landsat
883 satellite imagery. *Journal of maps*, 9(3): 456-473
- 884 Storrar, R.D., Stokes, C.R. and Evans, D.J. (2014a) Morphometry and pattern of a large sample (>
885 20,000) of Canadian eskers and implications for subglacial drainage beneath ice
886 sheets. *Quaternary Science Reviews*, 105: 1-25
- 887 Storrar, R.D., Stokes, C.R. and Evans, D.J. (2014b) Increased channelization of subglacial drainage
888 during deglaciation of the Laurentide Ice Sheet. *Geology*, 42(3): 239-242
- 889 Stroeven, A. P., Hättestrand, C., Kleman, J., Heyman, J., Fabel, D., Fredin, O., Goodfellow, B. W.,
890 Harbor, J. M., Jansen, J. D., Olsen, L., Caffee, M. W., Fink, D., Lundqvist, J., Rosqvist, G.
891 C., Strömberg, B. & Jansson, K. N. (2016) Deglaciation of Fennoscandia. *Quaternary
892 Science Reviews*, 147, 91-121.
- 893 Walther, J. (1894) Einleitung in die Geologie als historische Wissenschaft. In *Lithogenesis der
894 Gegenwart*. Jena: G. Fischer, Bd. 3: 535–1055.
- 895 Warren, W.P. and Ashley, G.M. (1994) Origins of the ice-contact stratified ridges (eskers) of
896 Ireland. *Journal of Sedimentary Research*, 64(3a): 433-449
- 897 Wilson, P., Ballantyne, C.K., Benetti, S., Small, D., Fabel, D. and Clark, C.D. (2019) Deglaciation
898 chronology of the Donegal Ice Centre, north-west Ireland. *Journal of Quaternary Science*,
899 34(1): 16-28
- 900 Winsemann, J., Asprion, U., Meyer, T. and Schramm, C. (2007) Facies characteristics of Middle
901 Pleistocene (Saalian) ice-margin subaqueous fan and delta deposits, glacial Lake Leine, NW
902 Germany. *Sedimentary Geology*, 193(1-4): 105-129

- 903 Winsemann, J., Hornung, J.J., Meinsen, J., Asprien, U., Polom, U., Brandes, C., BUßMANN,
904 M.I.C.H.A.E.L. and Weber, C. (2009) Anatomy of a subaqueous ice-contact fan and delta
905 complex, Middle Pleistocene, North-west Germany. *Sedimentology*, 56(4): 1041-1076
- 906 Winsemann, J., Lang, J., Polom, U., Loewer, M., Igel, J., Pollok, L. and Brandes, C. (2018) Ice-
907 marginal forced regressive deltas in glacial lake basins: geomorphology, facies variability
908 and large-scale depositional architecture. *Boreas*, 47(4): 973-1002
- 909 Wright, A. P., Siegert, M. J., Le Brocq, A. M., & Gore, D. B. (2008). High sensitivity of subglacial
910 hydrological pathways in Antarctica to small ice-sheet changes. *Geophysical Research*
911 *Letters*, 35(17), 1–5. <https://doi.org/10.1029/2008GL034937>
- 912 Zwally, H.J., Abdalati, W., Herring, T., Larson, K., Saba, J. and Steffen, K. (2002) Surface melt-
913 induced acceleration of Greenland ice-sheet flow. *Science*, 297(5579): 218-222
- 914
- 915



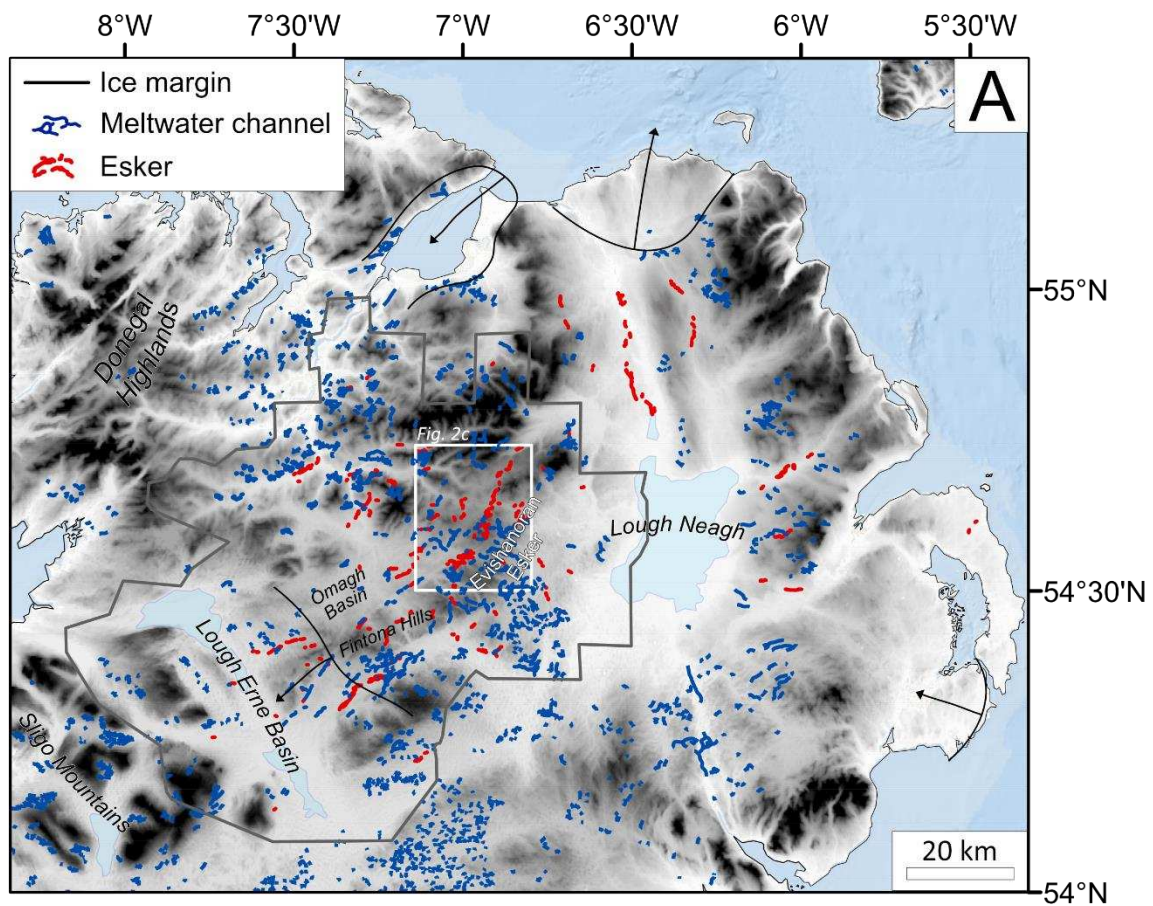
916

917 Figure 1. The distribution of mapped glacial landforms within the BRITICE v2 database across
 918 Northern Ireland (Clark *et al.*, 2018). Lineations include Mega-Scale Glacial Lineations (MSGL) and
 919 drumlins. Major ice flow directions during the LGM are indicated by the black arrows. The white box
 920 indicates the study area.

Facies type	Radar facies example	Facies characteristics	Facies interpretation
Esker ridge facies		Radar Facies 1: Chaotic, discontinuous reflectors.	Coarse gravel deposited subglacially under high flow velocities (Burke <i>et al.</i> , 2015)
		Radar Facies 2: Sub-horizontal moderately continuous reflectors	Vertical accretion of sandy material (Burke <i>et al.</i> , 2012)
		Radar Facies 3: Low-angle dipping reflections	Delta foresets composed of sand and gravel (Burke <i>et al.</i> , 2010)
		Radar Facies 4: Concave-up, bowl-shaped reflectors	Erosional trough fills (Perkins <i>et al.</i> , 2016)
Post-glacial facies		Radar Facies 5: Attenuated, horizontal reflections	Post-glacial peat infill (Jol and Smith, 1991)

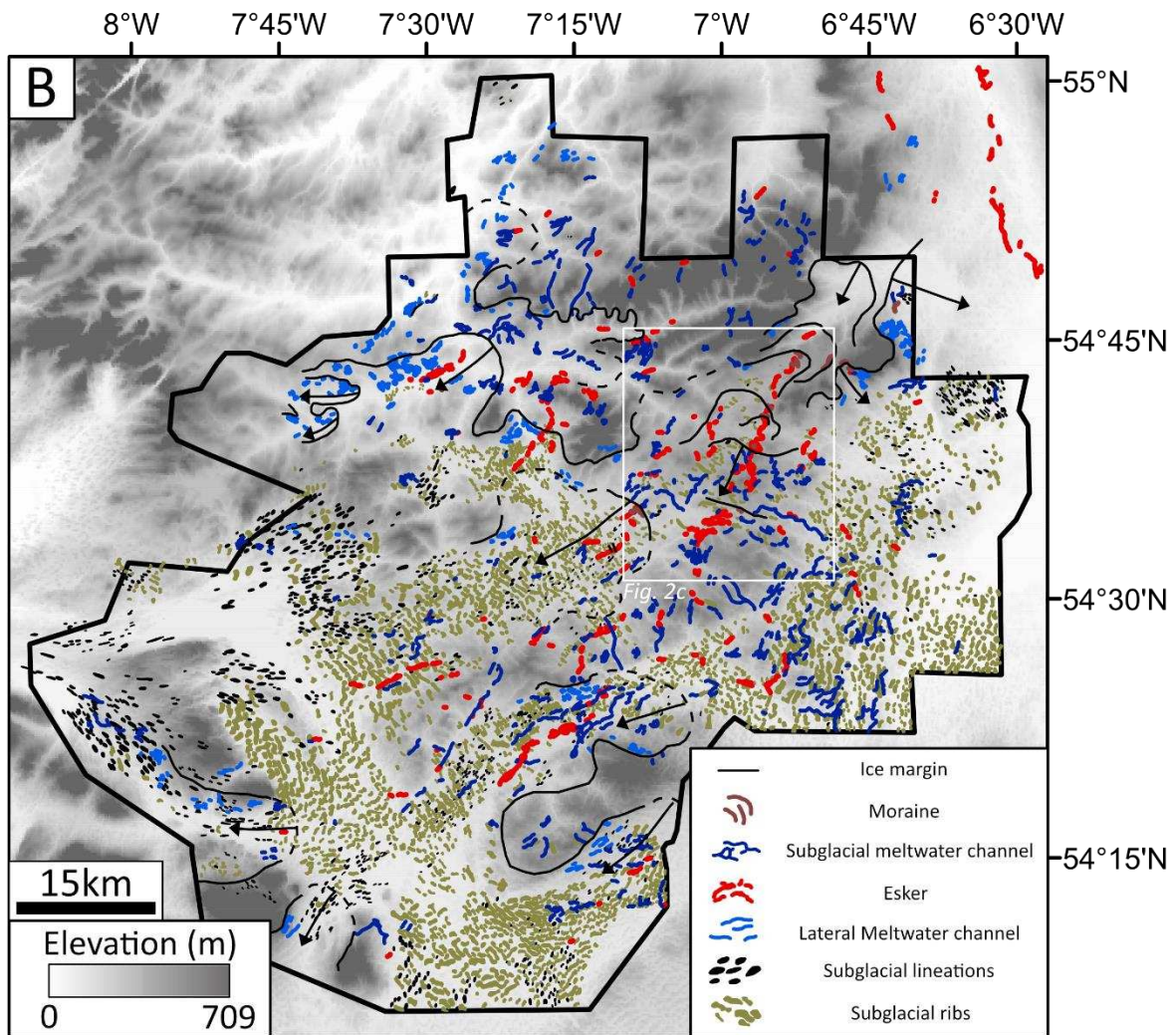
921

922 Table 1. Summary of key radar facies observed along the Evishanoran Esker, including both
923 glaciofluvial and post-glacial features. Further description and interpretation of radar facies is presented
924 in Section 4.2.1.



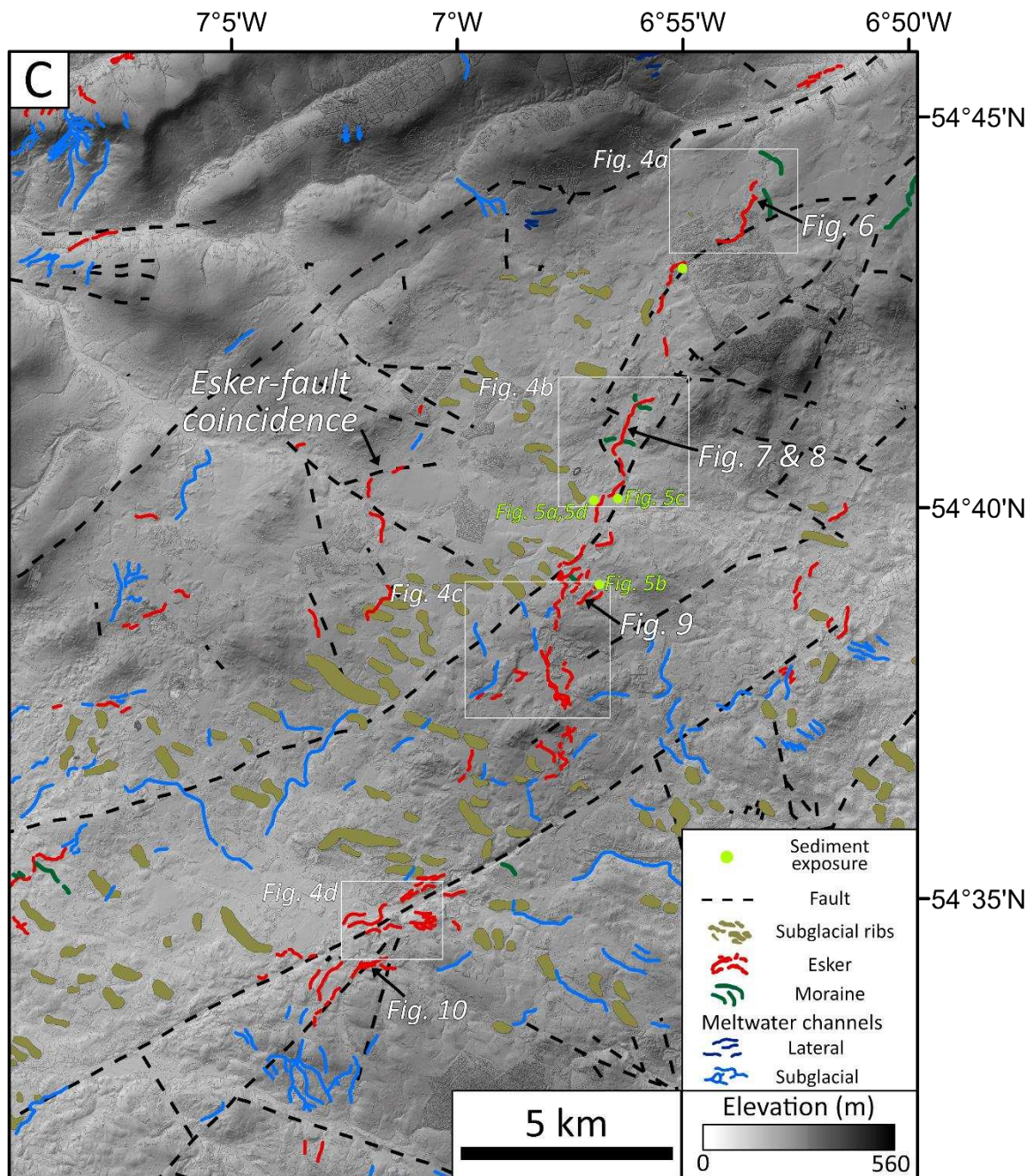
925

926 Figure 2. (a) An updated map of the meltwater landforms of Northern Ireland, including features
 927 mapped in this study. Meltwater channels from the BRITICE v2 compilation are also included (Clark
 928 *et al.*, 2018). Note the occurrence of a large esker system to the west of Lough Neagh, unreported in the
 929 BRITICE database. Ice margin positions are adapted from Greenwood and Clark (2009b), with arrows
 930 showing ice margin retreat direction. The grey box indicates the extent of high-resolution (~0.4 m)
 931 DSM coverage used within this study and shown in Figure 2b.



932

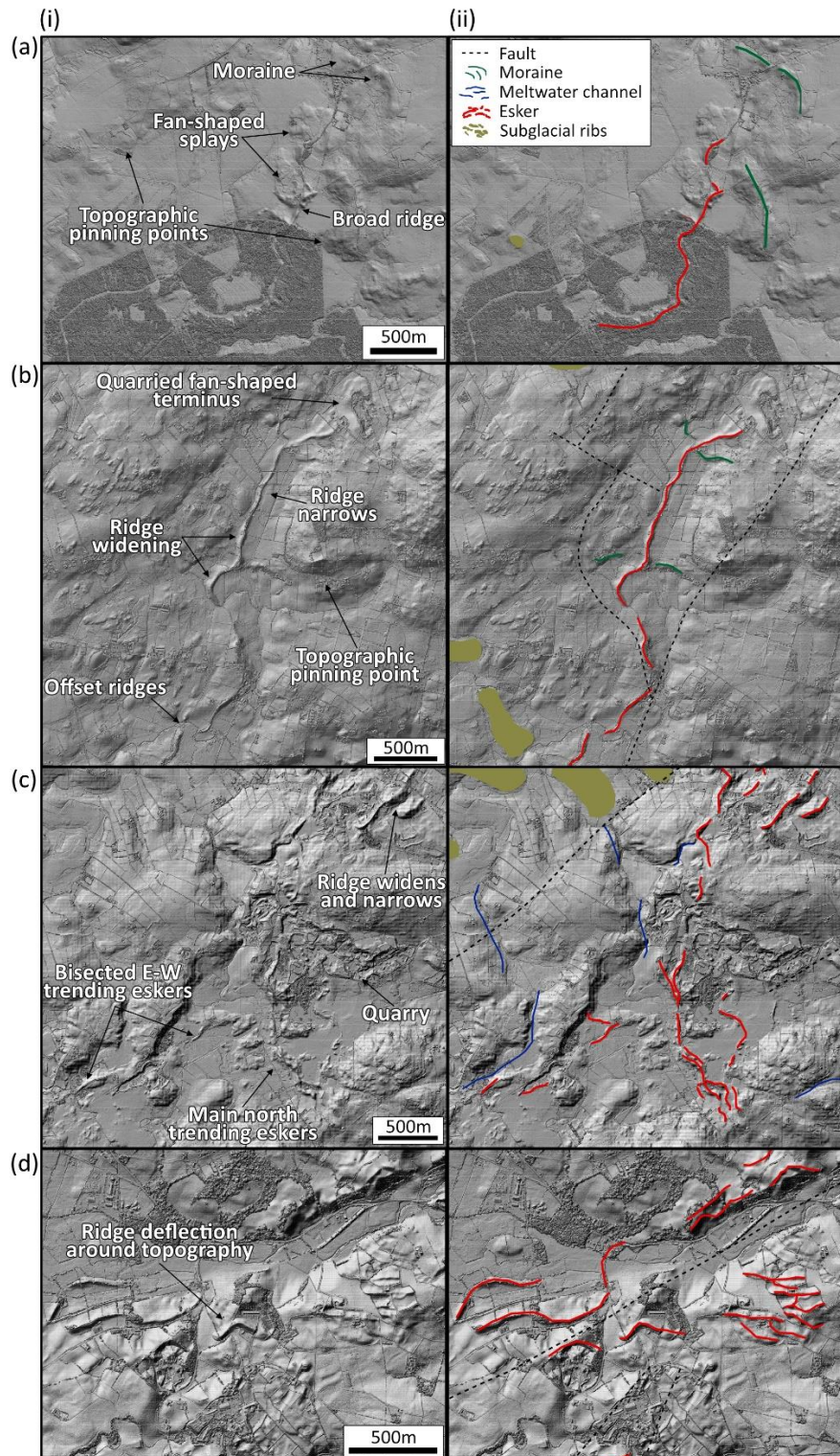
933 Figure 2. (b) Glacial geomorphology of SW Northern Ireland based on a 0.4m DSM. Schematic ice
 934 margin positions (black lines) have been drawn based on esker morphology, fan deposits, lateral
 935 meltwater channels and moraines. Dashed black lines indicate areas of lower certainty in ice margin
 936 position. Black arrows indicate ice margin retreat directions. The black outline indicates the extent of
 937 DSM coverage.



938
 939 Figure 2. (c) The esker system in County Tyrone, annotated with the location of investigated sediment
 940 exposures. Note the coincidence of the southern esker system with a large SW-NE trending fault, while
 941 some eskers in the northwest demonstrate dramatic changes in orientation to follow fault lines. White
 942 boxes highlight features detailed within Figure 4. Yellow text indicates which photographs from Figure
 943 5 relate to each sediment exposure. Geological faulting data is based on the 10K geology dataset,
 944 reproduced with the permission of the Geological Survey of Northern Ireland. Crown Copyright 2018.



945
 946 Figure 3. Photographs detailing the morphology of the Evishanoran Esker. (A) Looking east along a
 947 round-crested ridge within the complex, multi-ridge esker in the southern sector (54.571°N , -7.041°E).
 948 (B) An esker ridge ending in a fan-shaped deposit within the central sector of the esker complex, formed
 949 by water flow down the hill from the right of the image (54.650°N , -6.953°E). (C) A ridge along the
 950 Esker Road within the northern sector (54.683°N , -6.942°E). Radar surveys revealed peat infilling
 951 around the ridge, masking the true esker size. (D) Variations in ridge morphology towards the
 952 termination of the northern sector (54.734°N , -6.893°E).

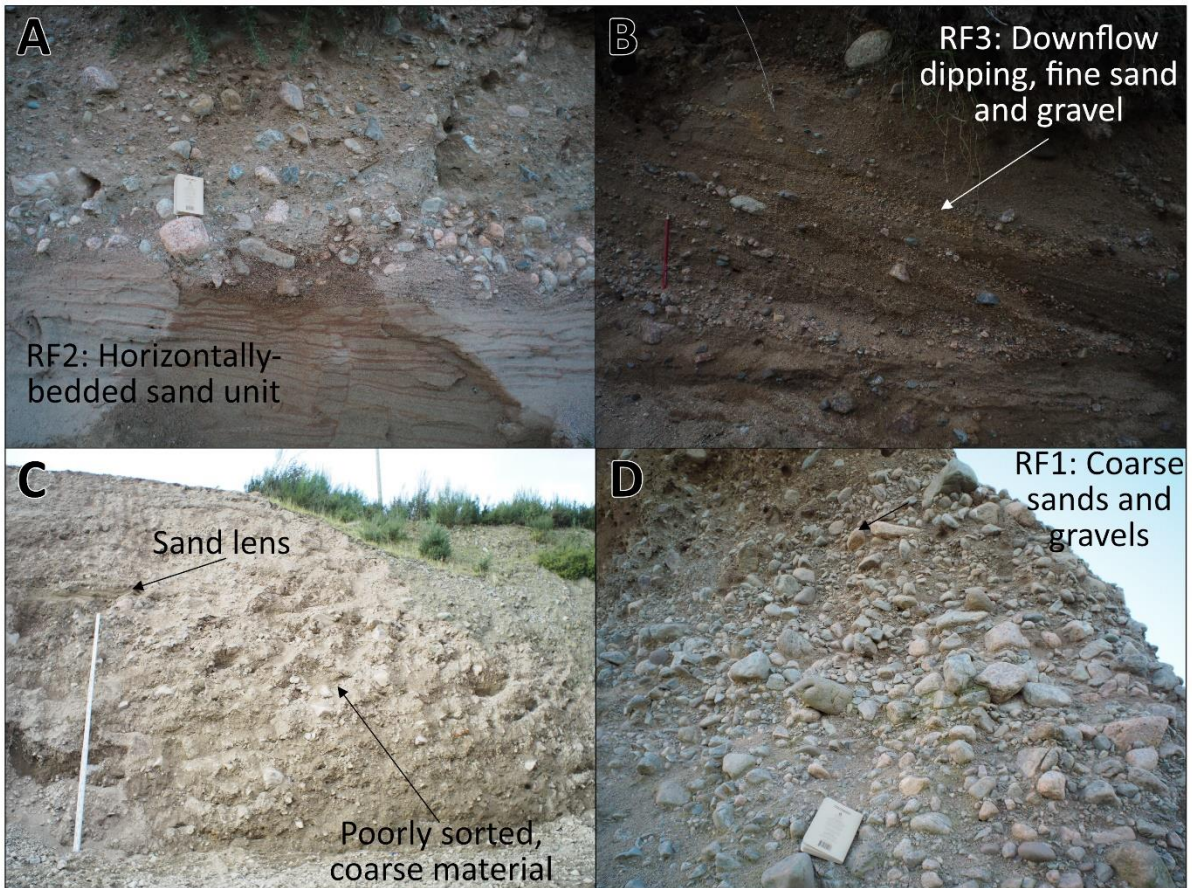


953

954 Figure 4. Hillshaded DEM detailing key morphological characteristics of the Evishanoran Esker. (a)
 955 Widening of the esker ridge towards the terminus of the simple system in the northern sector, (b) Offset
 956 ridges at the initiation of the simple system in the northern sector, (c) Cross-cutting of east trending
 957 ridges by the main north trending ridge within the complex esker system in the central sector of the
 958 esker complex, (d) Deflection of ridges around a topographic obstacle (possible bedrock or earlier
 959 drumlin) within the southern sector.

	Southern sector	Central sector	Northern sector
Planform	Complex, multi-ridge	Complex, tributary system	Simple
Average ridge length (m)	357	334	678
Sinuosity	1.17	1.21	1.20
Topographic context	Normal slope through undulating topography	Normal slope through hilly topography	Reverse slope through a uniform valley bottom
Relative relief (m)	~7	~6	~10-15
Total esker length (km)	~6.5 (36 ridges)	~7.4 (39 ridges)	~9.3 (10 ridges)

960 Table 2. The key morphological characteristics of the complex esker system in County Tyrone. The
961 distance along the crestline of each ridge was measured to define the average ridge length. Esker
962 sinuosity was calculated for each individual ridge by dividing the esker ridge length by the straight-line
963 distance from esker initiation to terminus, and is presented as a mean for each sector.



964

965

966

967

968

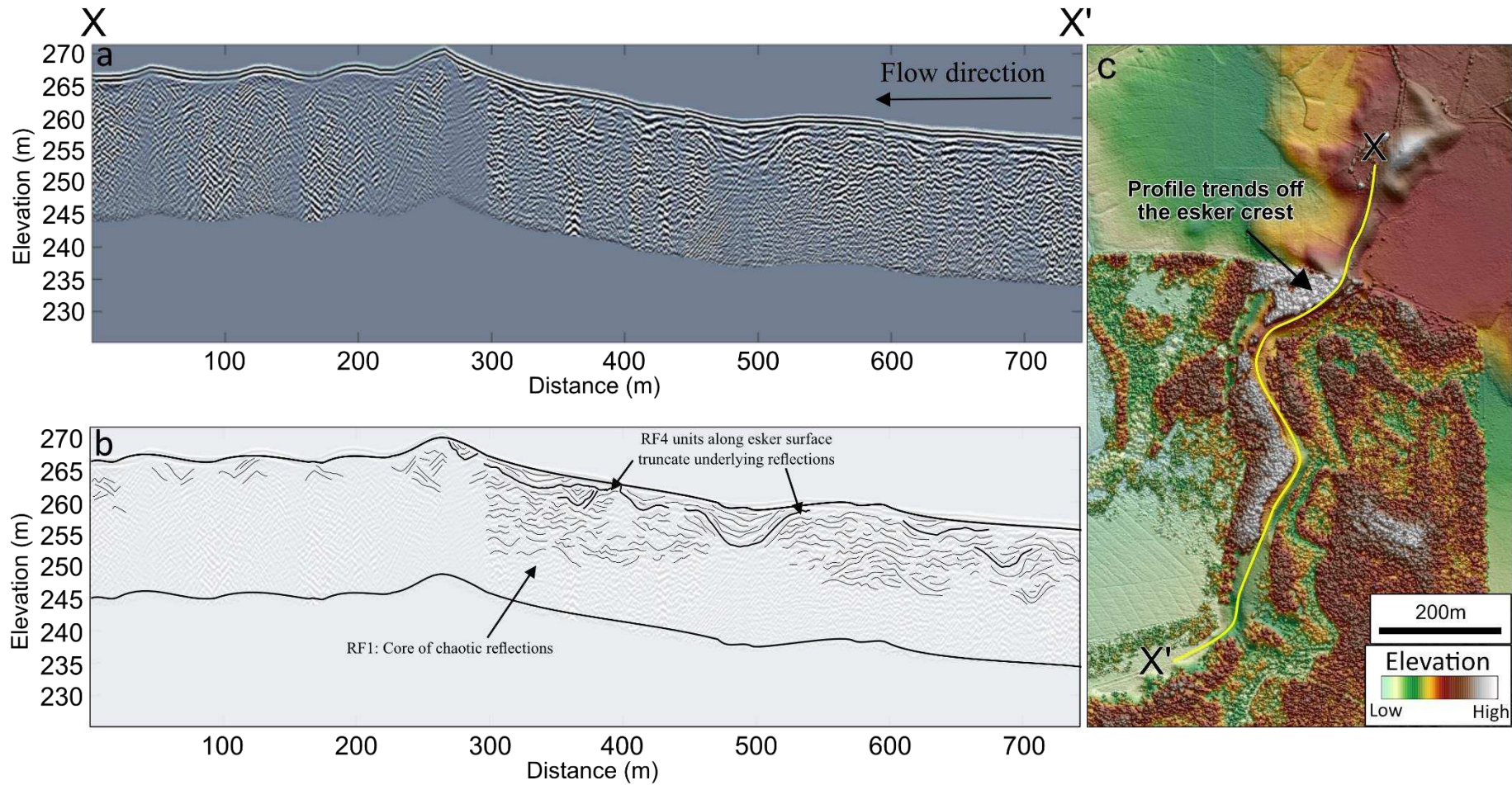
969

970

971

972

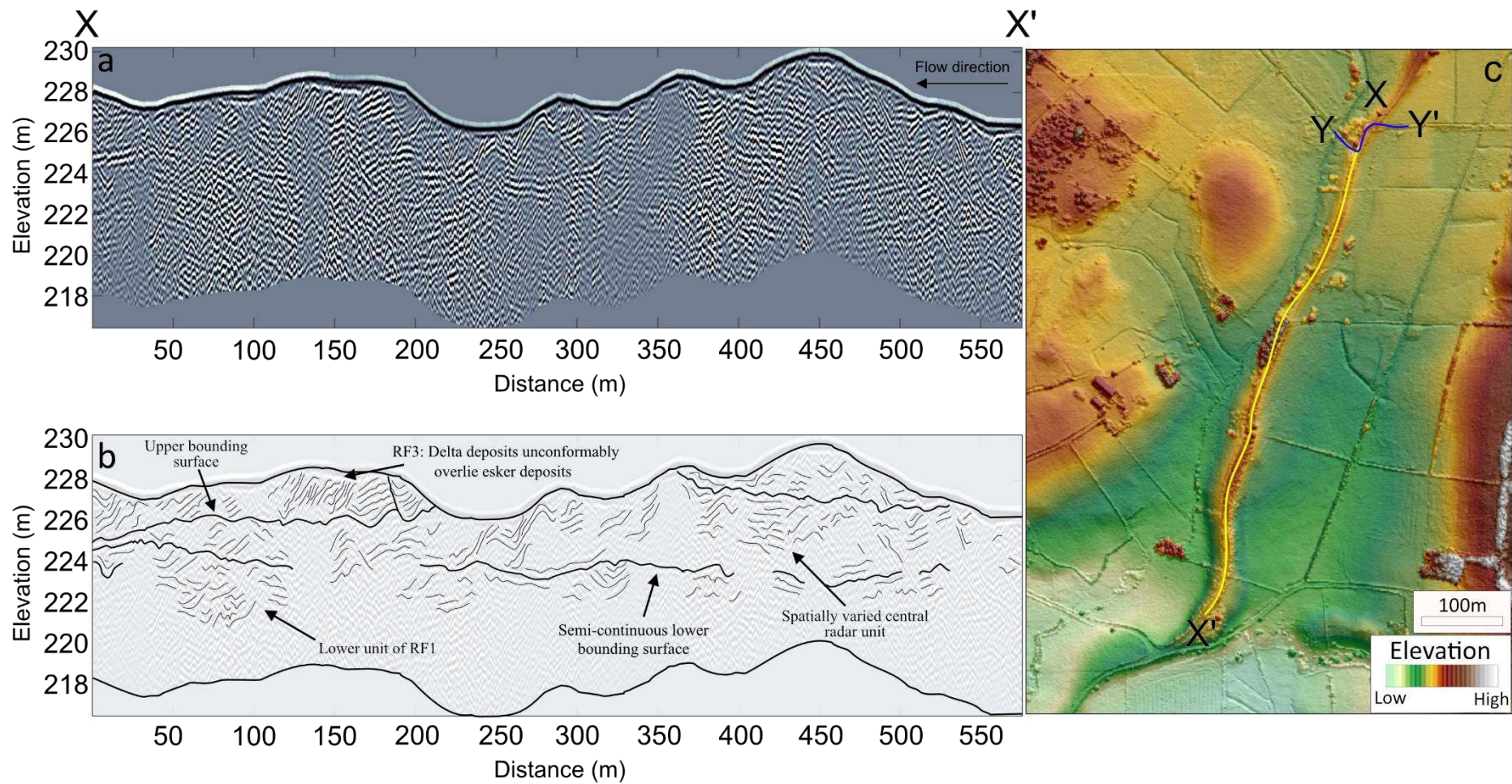
Figure 5. (a) Sediment exposure from the southern-end of the northern sector, consisting of a series of horizontally stratified sands (RF2), overlain by a poorly sorted sand and gravel unit (54.668°N, -6.950°E). (b) Sediment exposure within the central, complex esker system, dominated by a series of downflow-dipping sands and gravelly sands associated with RF3 (54.650°N, -6.953°E). (c) Quarried section of the single esker ridge system to the north of (a). Facies consist of coarse, diamictic material with boulders up to 50 cm (54.672°N, -6.941°E). (d) Poorly-sorted sand and gravel units observed within the northern sector, commonly associated with RF1 (54.668°N, -6.950°E).



973

974 Figure 6. (a) 100 MHz long-profile radar survey along the crest of a single ridge esker towards the NE terminus of the County Tyrone Esker, the location of the
 975 survey line is presented in Figure 2. Ice flow direction is indicated by the black arrow. (b) shows an interpreted radar profile derived through the tracing of key
 976 reflections. (c) Inset figure showing the detailed esker morphology and the location of radar survey (yellow line).

977

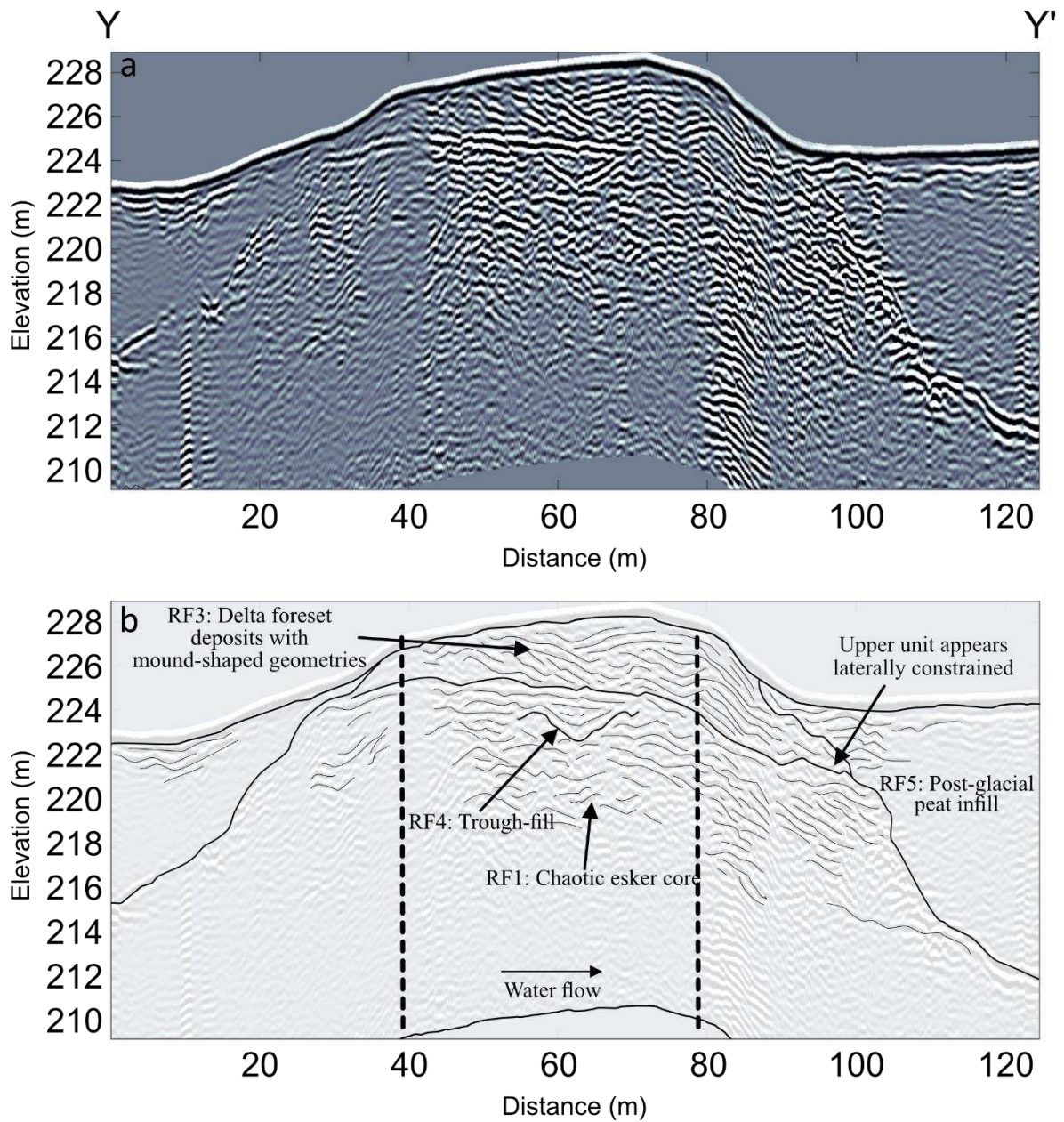


978

979 Figure 7. (a) 160 MHz long-profile radar survey along the crest of a single ridge esker near the initiation of the simple system, the location of the survey line is
 980 presented in Figure 2. Ice flow direction is indicated by the black arrow. (b) shows an interpreted radar profile derived through the tracing of key reflections.

981 (c) Inset figure showing the detailed esker morphology and the location of radar surveys for Figure 7 (yellow line) and Figure 8 (blue line).

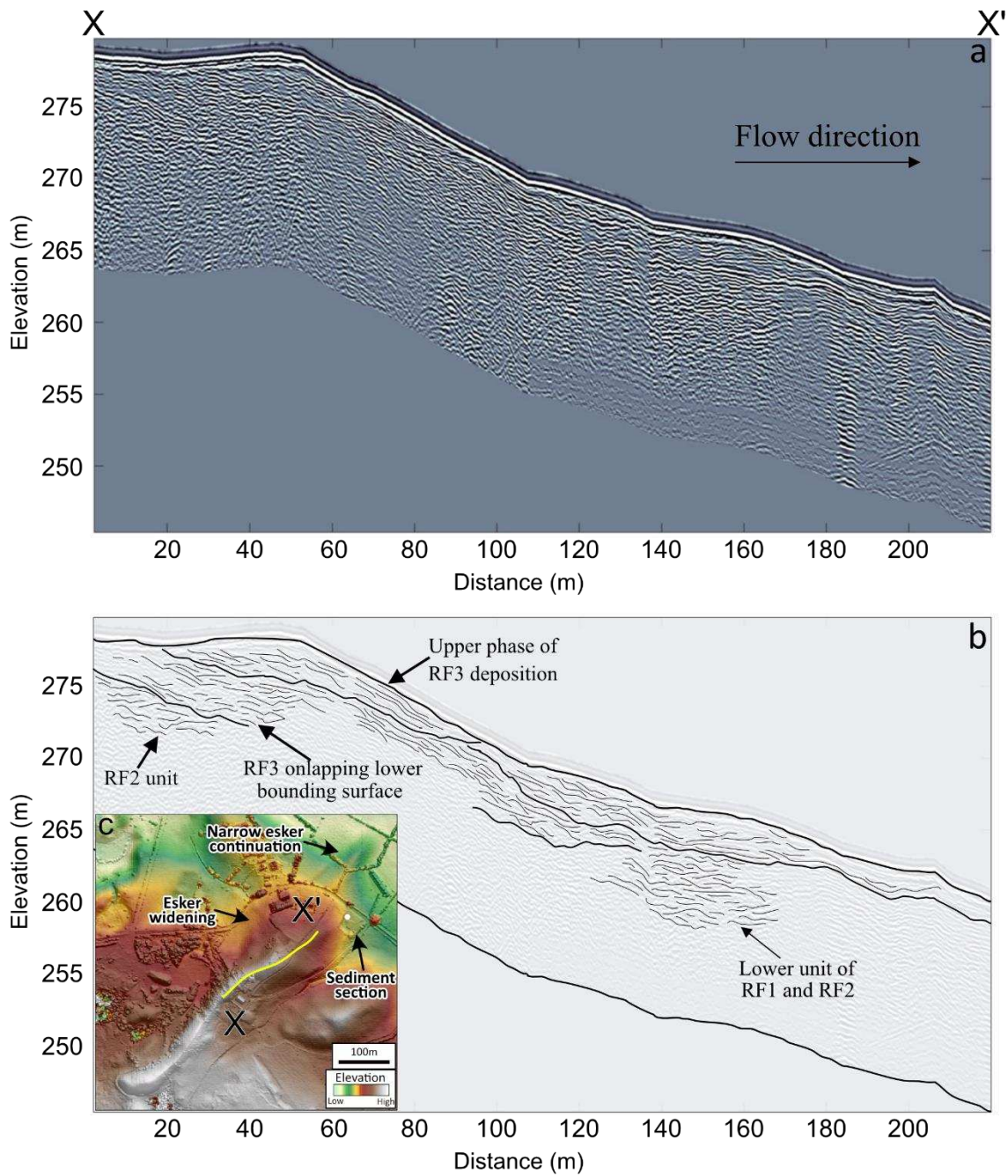
982



983

984 Figure 8. (a) 160 MHz cross-profile radar survey of a single ridge esker near the initiation of the northern
 985 sector. (b) shows an interpreted radar profile derived through the tracing of key reflections. Vertical
 986 dashed lines indicate the portion of the radar survey which travelled along the esker ridge. The location
 987 of the radar profile is indicated on Figure 7c by a blue line.

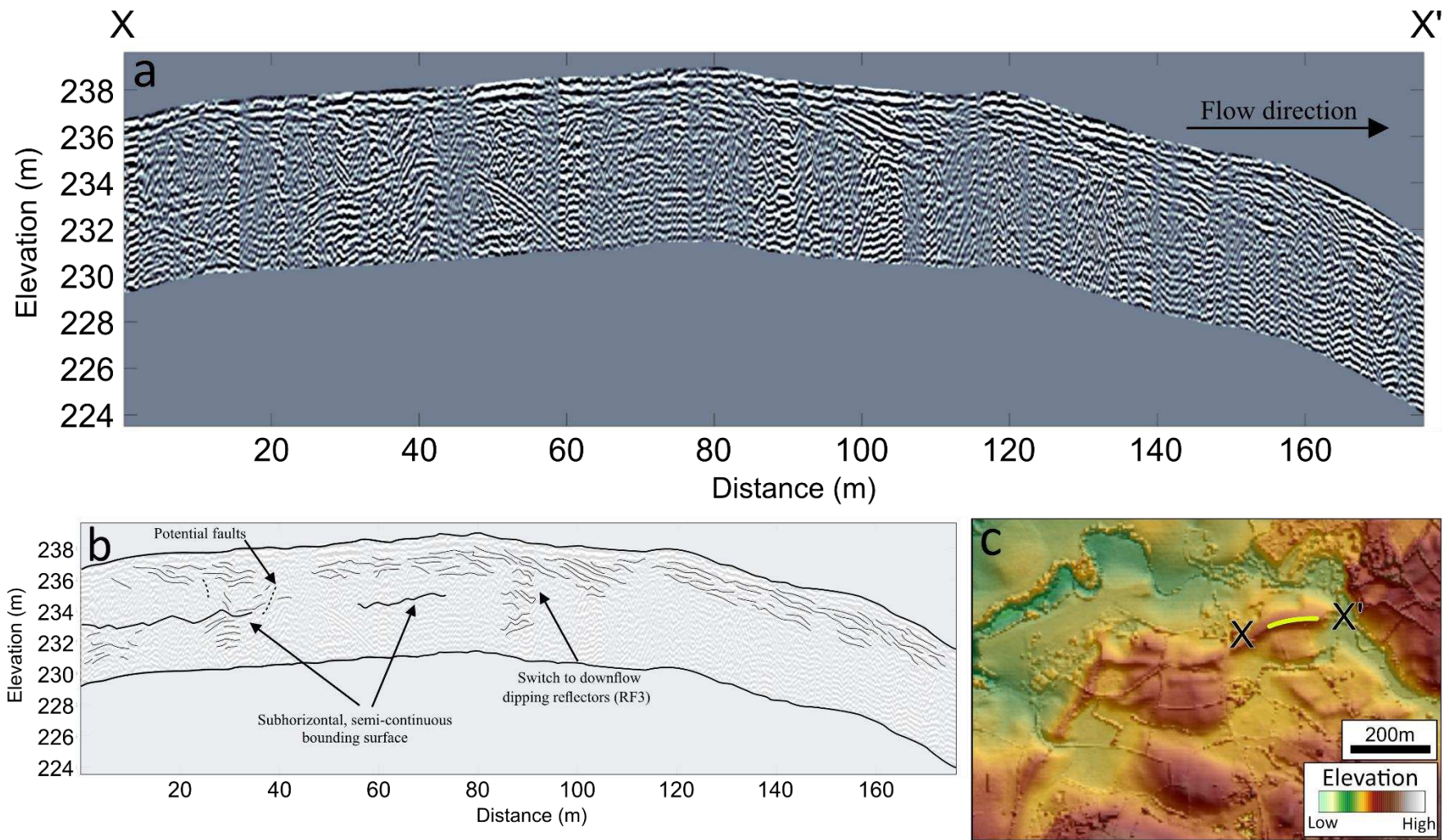
988



989

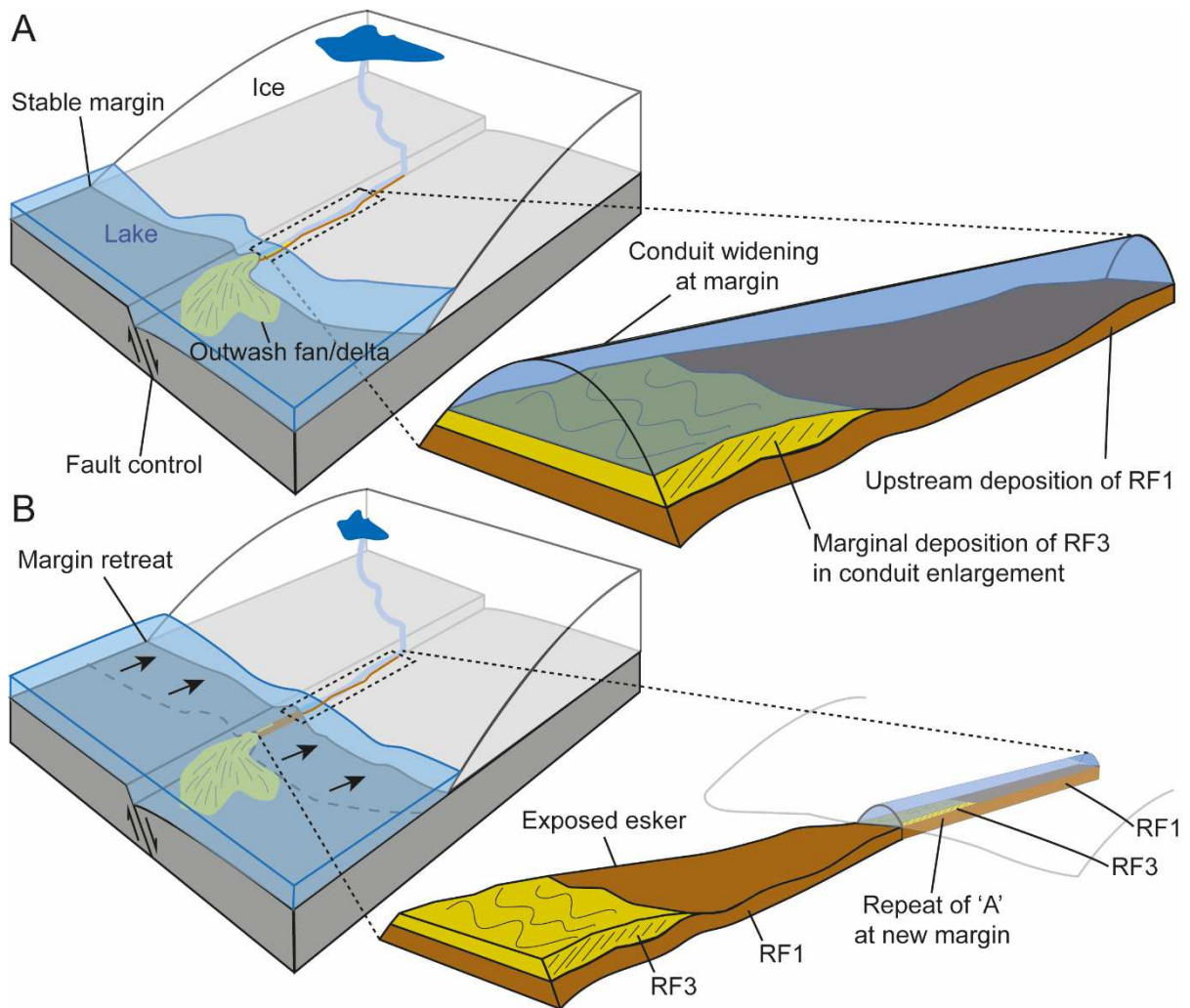
990 Figure 9. (a) 160 MHz radar profile along the crest of an esker within the complex central sector. Ice
 991 flow direction is indicated by the black arrow. (b) shows an interpreted radar profile derived through
 992 the tracing of key reflections. (c) Inset figure showing the detailed esker morphology and the location
 993 of radar survey (yellow line), while the labelled sediment section (white dot) is photographed in Figure
 994 5b.

995



996

997 Figure 10. (a) 160 MHz radar profile along the crest of an esker within the southern sector. Ice flow direction is indicated by the black arrow. (b) shows an
 998 interpreted radar profile derived through the tracing of key reflections. (c) Inset figure showing the detailed esker morphology and the location of radar survey
 999 (yellow line).



1000

1001 Figure 11. A conceptual model of the time-transgressive esker deposition. (a) Delta foresets are
 1002 deposited in a proglacial lake at the ice sheet margin due to conduit widening, while coarser material is
 1003 deposited up-ice in the subglacial conduit. (b) Ice margin retreat leads to the deposition of foresets on
 1004 top of the core of esker material.